AD-A131 431 HIGH-LATITUDE AND EQUATORIAL RESEARCH SUPPORT FOR PREDICTING HIGH-ALTITUD..(U) SRI INTERNATIONAL MENLO PARK CA C L RINO ET AL. 01 AUG 82 DNA-TR-81-176 1/1

UNCLASSIFIED DNA001-81-C-0076 F/G 4/1 NL

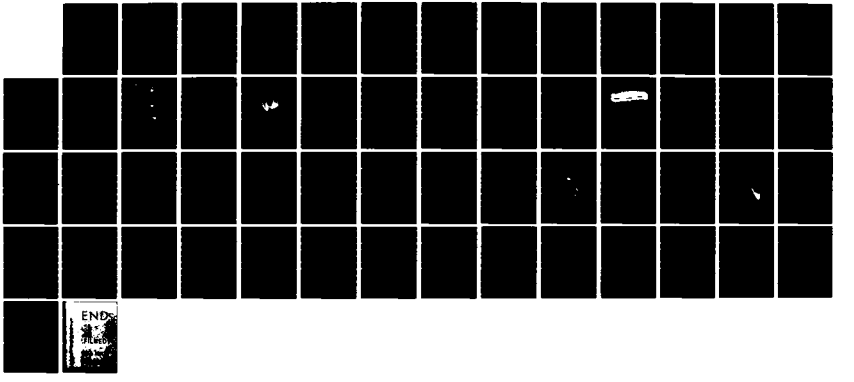

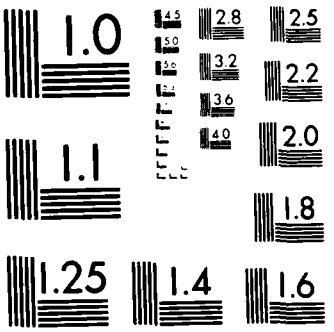

MICROCOPY RESOLUTION TEST CHART
NATIONAL BUREAU OF STANDARDS 1963 A

(12)

DNA-TR-81-176

HIGH-LATITUDE AND EQUATORIAL RESEARCH SUPPORT FOR PREDICTING HIGH-ALTITUDE NUCLEAR EFFECTS

Charles L. Rino
James F. Vickrey
Robert C. Livingston
Roland T. Tsunoda
SRI International
333 Ravenswood Avenue
Menlo Park, California 94025

1 August 1982

Technical Report

CONTRACT No. DNA 001-81-C-0076

APPROVED FOR PUBLIC RELEASE;
DISTRIBUTION UNLIMITED.

THIS WORK WAS SPONSORED BY THE DEFENSE NUCLEAR AGENCY
UNDER RDT&E RMSS CODE B322081466 S99QAXHC00022 H2590D.

Prepared for
Director
DEFENSE NUCLEAR AGENCY
Washington, DC 20305

Destroy this report when it is no longer needed. Do not return to sender.

PLEASE NOTIFY THE DEFENSE NUCLEAR AGENCY, ATTN: STTI, WASHINGTON, D.C. 20305, IF YOUR ADDRESS IS INCORRECT, IF YOU WISH TO BE DELETED FROM THE DISTRIBUTION LIST, OR IF THE ADDRESSEE IS NO LONGER EMPLOYED BY YOUR ORGANIZATION.

UNCLASSIFIED

SECURITY CLASSIFICATION OF THIS PAGE *(When Data Entered)*

REPORT DOCUMENTATION PAGE

READ INSTRUCTIONS BEFORE COMPLETING FORM

1. REPORT NUMBER: DNA-TR-81-176	2. GOVT ACCESSION NO.
3. RECIPIENT'S CATALOG NUMBER	
4. TITLE *(and Subtitle)*: HIGH-LATITUDE AND EQUATORIAL RESEARCH SUPPORT FOR PREDICTING HIGH-ALTITUDE NUCLEAR EFFECTS	5. TYPE OF REPORT & PERIOD COVERED: Technical Report
	6. PERFORMING ORG. REPORT NUMBER: SRI Project 2623
7. AUTHOR(s): Charles L. Rino, James F. Vickrey, Robert C. Livingston, Roland T. Tsunoda	8. CONTRACT OR GRANT NUMBER(s): DNA 001-81-C-0076
9. PERFORMING ORGANIZATION NAME AND ADDRESS: SRI International, 333 Ravenswood Avenue, Menlo Park, California 94025	10. PROGRAM ELEMENT, PROJECT, TASK AREA & WORK UNIT NUMBERS: Task S99QAXHC-00022
11. CONTROLLING OFFICE NAME AND ADDRESS: Director, Defense Nuclear Agency, Washington, D.C. 20305	12. REPORT DATE: 1 August 1982
	13. NUMBER OF PAGES: 54
14. MONITORING AGENCY NAME & ADDRESS *(if different from Controlling Office)*	15. SECURITY CLASS *(of this report)*: UNCLASSIFIED
	15a. DECLASSIFICATION/DOWNGRADING SCHEDULE: N/A since Unclassified

16. DISTRIBUTION STATEMENT *(of this Report)*

Approved for public release; distribution unlimited.

17. DISTRIBUTION STATEMENT *(of the abstract entered in Block 20, if different from Report)*

18. SUPPLEMENTARY NOTES

This work was sponsored by the Defense Nuclear Agency under RDT&E RMSS Code B322081466 S99QAXHC00022 H2590D.

19. KEY WORDS *(Continue on reverse side if necessary and identify by block number)*

Equatorial Spread F

Striations

Auroral Phenomenology

20. ABSTRACT *(Continue on reverse side if necessary and identify by block number)*

This report summarizes the high-latitude and the equatorial natural ionospheric research support that has been conducted to improve and extend high-altitude nuclear predictive capability. This work marks the formal completion of the equatorial research effort. That effort has been very successful and the results are summarized in detail. The primary future effort will be directed toward auroral phenomena. The preliminary work in this area is described in the report.

DD FORM 1 JAN 73 1473 EDITION OF 1 NOV 65 IS OBSOLETE

UNCLASSIFIED

SECURITY CLASSIFICATION OF THIS PAGE *(When Data Entered)*

TABLE OF CONTENTS

Section		Page
	LIST OF ILLUSTRATIONS	2
I	INTRODUCTION	5
II	HIGH-LATITUDE STRUCTURE	7
III	EQUATORIAL STRUCTURE	18
	A. Large-Scale Structure (Greater than 10 km	18
	B. Intermediate-Scale Structure (10 km to 100 m)	34
	C. Transitional-Scale Structure (100 m to 10 m)	35
	D. Small-Scale Structure (Less than 10 m)	38
IV	DISCUSSION AND CONCLUSIONS	44
	REFERENCES	47

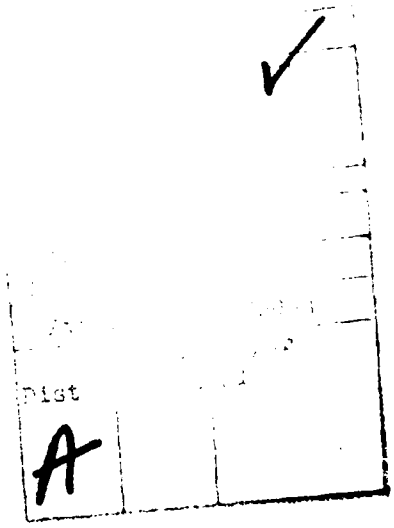

LIST OF ILLUSTRATIONS

Figure		Page
1	Meridional Electron-Density Profile Showing Structured F-Region Plasma Enhancements, "Blobs"	9
2	Simulation of the Nonlinear Evolution of Convective Instability for Auroral-Zone Geometry	10
3	Chatanika Radar Reconstruction of Transverse Electron Density Profile Showing East-West Structure	12
4	Morphology of Irregularity Anisotropy Under Conditions of Moderate Activity.	14
5	Schematic Diagram of Anisotropy Variation and Its Relation to Average Nighttime Convection Pattern.	15
6	Model Computation of Diffusive Decay of Kilometer-Scale Irregularities.	16
7	Evidence of Wave Structure in Contours of Constant Electron Density Found in the Bottomside F Layer Before the Development of ESF Backscatter.	20
8	Sequence of ALTAIR Backscatter Maps Showing Three Upwellings That Develop ESF Backscatter Along Their West Walls, Followed by Plume Development	21
9	Contour Map Showing the Latitudinal Distribution of Electron Density Greater Than 2×10^5 el/cm^3 and the Magnetic-Field Alignment of the Plasma Depletion.	22
10	Sequence of ALTAIR Backscatter Maps That Show the Structuring of the West Wall of an Upwelling.	23
11	Simultaneous Measurements of F-Region Plasma Drift and Neutral Wind, Revealing a Significant Slip Velocity at Low Altitudes.	25

LIST OF ILLUSTRATIONS (concluded)

Figure		Page
12	Descriptive Model of Plasma Structuring in the Equatorial F Layer Produced by the Gradient-Drift and Collisional Rayleigh-Taylor Instabilities	26
13	Sequence of ALTAIR Backscatter Maps Showing the Development of ESF Plumes Without Large-Scale Upwellings in the Bottomside F Layer and the Distortion of Those Plumes by Velocity Shear.	28
14	Electron-Density Profile Obtained Along Radial Line in Figure 13(e).	29
15	Continuation of the Sequence of ALTAIR Backscatter Maps Shown in Figure 13	31
16	Example of an ESF Backscatter Plume That has Developed Without Any Bifurcation	32
17	ALTAIR Backscatter Map Showing Progressive Structuring of Backscatter Plume.	33
18	ESF In Situ Spectral Density Function Measured During DNA Plumex Experiment Campaign.	36
19	Measurements of Power-Law Index in Large-Scale and Small-Scale Spectral Regimes from DNA Plumex Rocket Campaign	37
20	Sequence of ALTAIR Backscatter Maps Showing the Decay Phase of an ESF Backscatter Plume	42

I INTRODUCTION

The relevance of naturally occurring F-region plasma instabilities for understanding the onset, the nonlinear evolution, and the ultimate decay of nuclear-induced striations is well established. Indeed, in lieu of actual nuclear data, naturally occurring striations such as those in the auroral and equatorial ionospheres provide the only means of accumulating large, high-quality data bases for verifying our understanding of these processes; moreover, the radio-wave propagation effects in the auroral and equatorial regions can degrade the performance of DoD systems.

The objective of the work conducted under this contract was to use our extensive auroral zone and equatorial data base to identify and measure in situ the parameters that affect the onset, nonlinear evolution, and decay of striations. The intensity and spectral characteristics of intermediate- and small-scale striations are most important because they disrupt radio-wave systems.

Investigations of equatorial spread-F (ESF) phenomena have made valuable contributions to this effort. Over the past five years, the Defense Nuclear Agency (DNA) has supported a number of field campaigns that have used extensively the ALTAIR and TRADEX radars. The commonality of the physical processes that structure F-region ionization in the equatorial and auroral zones (Ossakow, 1979) has been thoroughly exploited. The equatorial phenomena, however, are much more consistent in their development and evolution, evidently, because of the much broader variety (and variability) of auroral-zone phenomena that can affect the instability development. These include particle precipitation, a highly conducting E layer, and large convection velocities.

In Section II of this report, we review the high-latitude work that has been performed under this contract. This work includes analysis of

spaced-receiver data from the Wideband satellite experiment and the development of a theoretical framework for interpreting the global morphology of high-latitude scintillation. The model has been used to formulate a set of hypotheses that can be tested with data from the planned DNA polar satellite experiment.

Section III is an overview of all the experimental ESF work that has been performed under DNA programs. This contract is the conclusion of the equatorial experimental program for high-altitude nuclear-effects predictions. We expect that future equatorial programs will use the regular occurrence of ESF as a source of highly structured plasma with known spectral characteristics for systems tests, or testing new adaptations of the basic channel modeling method for evaluating the deleterious effects of propagation disturbances, or both.

In Section IV we discuss the ramifications of the results summarized in Sections II and III with regard to probable DoD needs.

II HIGH-LATITUDE STRUCTURE

An important finding from the Wideband satellite experiment was the nighttime scintillation enhancement that occurs with high probability whenever the propagation path lies within the plane of the local L shell (Fremouw et al., 1977; Rino et al., 1978). The phenomenon has been attributed to a geometrical enhancement from sheet-like irregularities. Evidence is accumulating, however, for a localized source region that also contributes to the nighttime scintillation enhancement. Through combined incoherent scatter and scintillation observations, the F-region source of the irregularities and the dynamics of the source region have been identified (Vickrey et al., 1980). Enhanced scintillations appear to be associated with the horizontal plasma-density gradients (or walls) of localized plasma-density enhancements, or (blobs), in the auroral F layer.

The experimental and theoretical work that has led to our current understanding of this high-latitude phenomenon is reviewed in Rino and Vickrey (1982). Because of the exceptionally good definition of the source region and its dynamics, we have concentrated our analysis efforts on this particular source of high-latitude irregularities.

Under active conditions in the nighttime sector of the auroral zone, the convection electric field has a westward component (southward drift). On this basis, a northward directed gradient is stable to the gradient-drift instability (e.g., Linson and Workman, 1970). This led Ossakow and Chaturvedi (1979) to propose the current-convective instability as the structuring mechanism. Field-aligned currents provide the free energy to destabilize the gradients that are otherwise stable to the gradient-drift instability. For typical observed values of field-aligned currents, however, this instability is not nearly as strong as the gradient-drift instability (e.g., Keskinen and Ossakow, 1982).

The unstable F-region blob, however, often has a much more complex structure than a single plasma enhancement. Figure 1 illustrates this and shows a meridional electron-density contour map made from a Chatanika radar elevation scan. Vickrey et al. (1980) have shown that scintillation enhancements occurred when the features marked (1) and (2) in the figure passed through the propagation path of the TRIAD satellite.

The main blob has alternating gradients associated with a large-scale modulation that was likely to have been imparted by the soft-electron precipitation source that generated the plasma-density enhancements. From this figure it is clear that some segment of the blob would be gradient-drift unstable, even without the help of destabilizing field-aligned currents.

The effects of the gradient-drift and current-convective instabilities are clearly evident in a recent numerical simulation of a two-sided plasma enhancement (Keskinen and Ossakow, 1982). In their model an electric field with components directed northward and westward are included, together with a typical field-aligned current. Figure 2 shows the plasma structure after evolution over 1600 s. The dominance of gradient-drift growth over current-convective growth is clearly evident. The dominant large-scale structuring occurred on the northern wall, which is gradient-drift unstable because of the presence of a westward electric-field component. The slight tilt in the interpenetrating low- and high-density regions is produced by velocity shear effects induced by the presence of the northward electric field component (e.g., Perkins and Doles, 1975). We note in passing that the large-scale structure is similar to those produced by the gravity-driven Rayleigh-Taylor instability in the equatorial ionosphere (see Section III).

As with all numerical simulations that accurately model the macro-scale structures, however, the above type of simulation does not retain sufficient resolution to preserve the intermediate- to small-scale structures that cause the scintillation enhancements. It is important, nonetheless, to verify that the structuring process is initiated at large scales. In this sense, it is necessary to determine whether east-

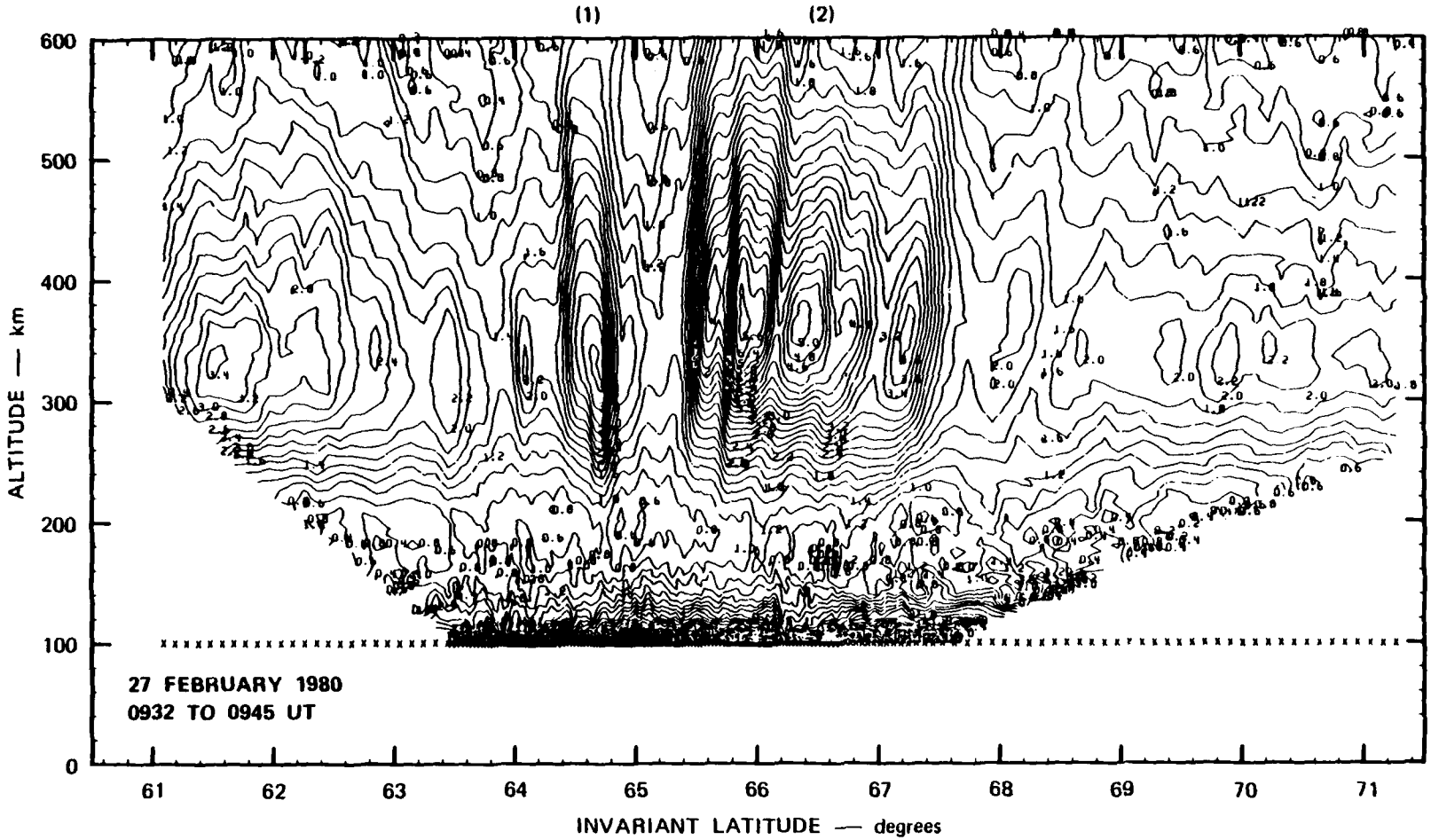

FIGURE 1 MERIDIONAL ELECTRON-DENSITY PROFILE SHOWING STRUCTURED F-REGION PLASMA ENHANCEMENTS, "BLOBS"

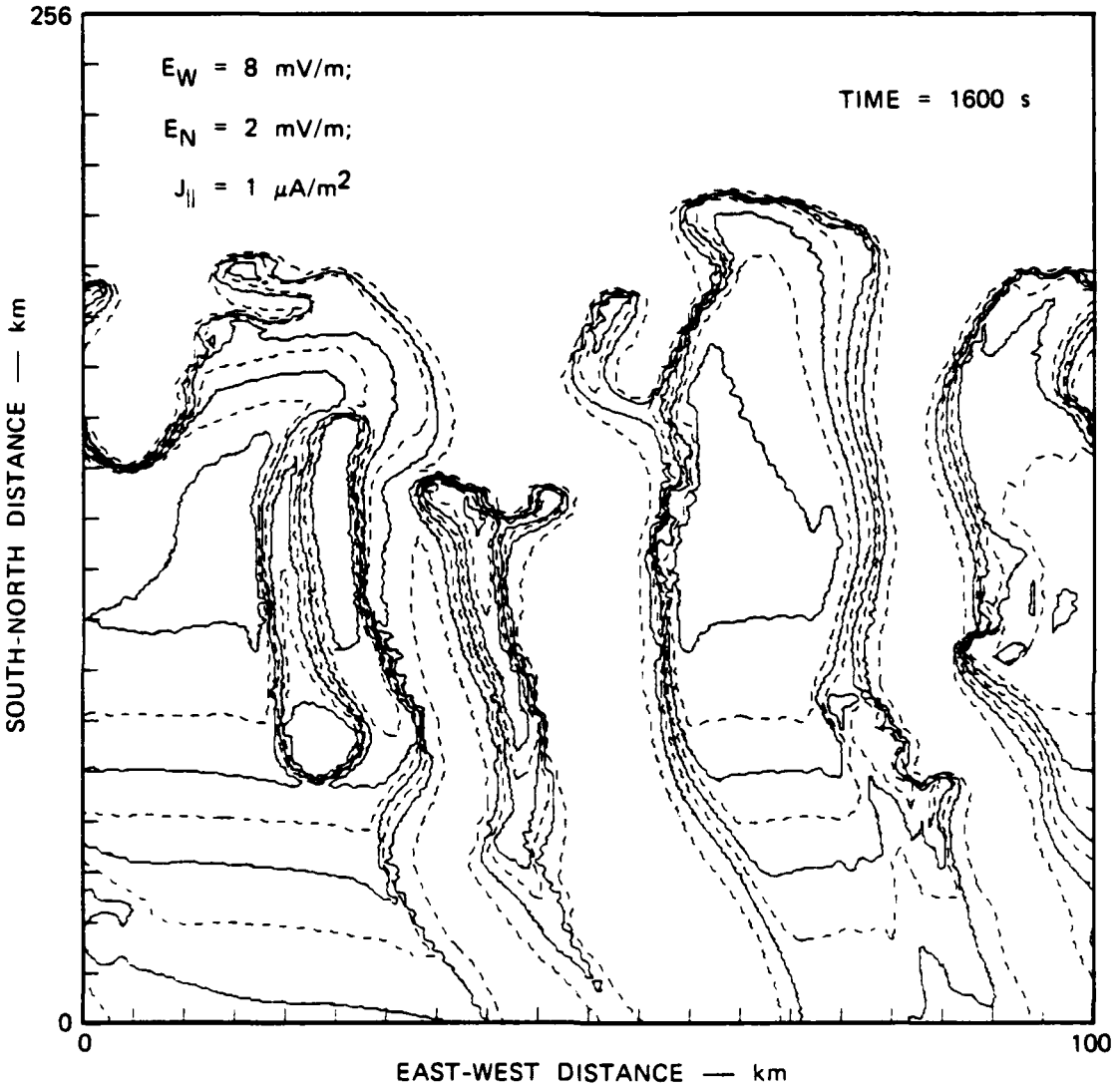

Source: Keskinan and Ossakow [1982]

FIGURE 2 SIMULATION OF THE NONLINEAR EVOLUTION OF CONVECTIVE INSTABILITY FOR AURORAL-ZONE GEOMETRY

west structure similar to those in Figure 2 are indeed observed in the auroral ionosphere.

Thus, under the current contract, in November 1981 a series of experiments were conducted using the Chatanika radar to map the large-scale blob structure in a horizontal plane transverse to the geomagnetic field. This was accomplished by combining the data from several rapid elevation scans. Figure 3 shows the preliminary results from one such measurement. These results, obtained in the local midnight sector, clearly show east-west structure along the southern boundary of an F-region blob. The generally northeast orientation of the mean southern boundary is most likely caused by the ionization source. The large-scale irregularities along the southern boundary was consistent with gradient-drift structuring by a southward blowing neutral wind. (In the event the east-west electric field was very small.)

Our preliminary results show that we have good semiquantitative agreement with the predicted nonlinear evolution of auroral-zone F-region-plasma enhancements. We have obtained a large data base, and detailed analysis is being pursued under a separate contract.

Turning now to the intermediate- to small-scale structure, we have performed a detailed analysis of the irregularity anisotropy as measured by the Wideband satellite spaced-receiver system operated at Poker Flat, Alaska. The measurement technique is described in Rino and Livingston (1982); the results of the analysis are described in Livingston et al. (1982).

By carefully measuring the variations of the axial ratio and orientation angle of the diffraction pattern during a large number of satellite passes, Livingston et al. (1982) were able to identify systematic transitions among three generic types of irregularity structures: rods, wings, and sheets. Rods are isotropic in the plane transverse to the geomagnetic field and can be characterized by an axial ratio (parallel to transverse dimensions) of a:1. Wings and sheets are elongated both along the geomagnetic field and in the transverse plane along the direction of the local L shell; hence, they are characterized by two axial

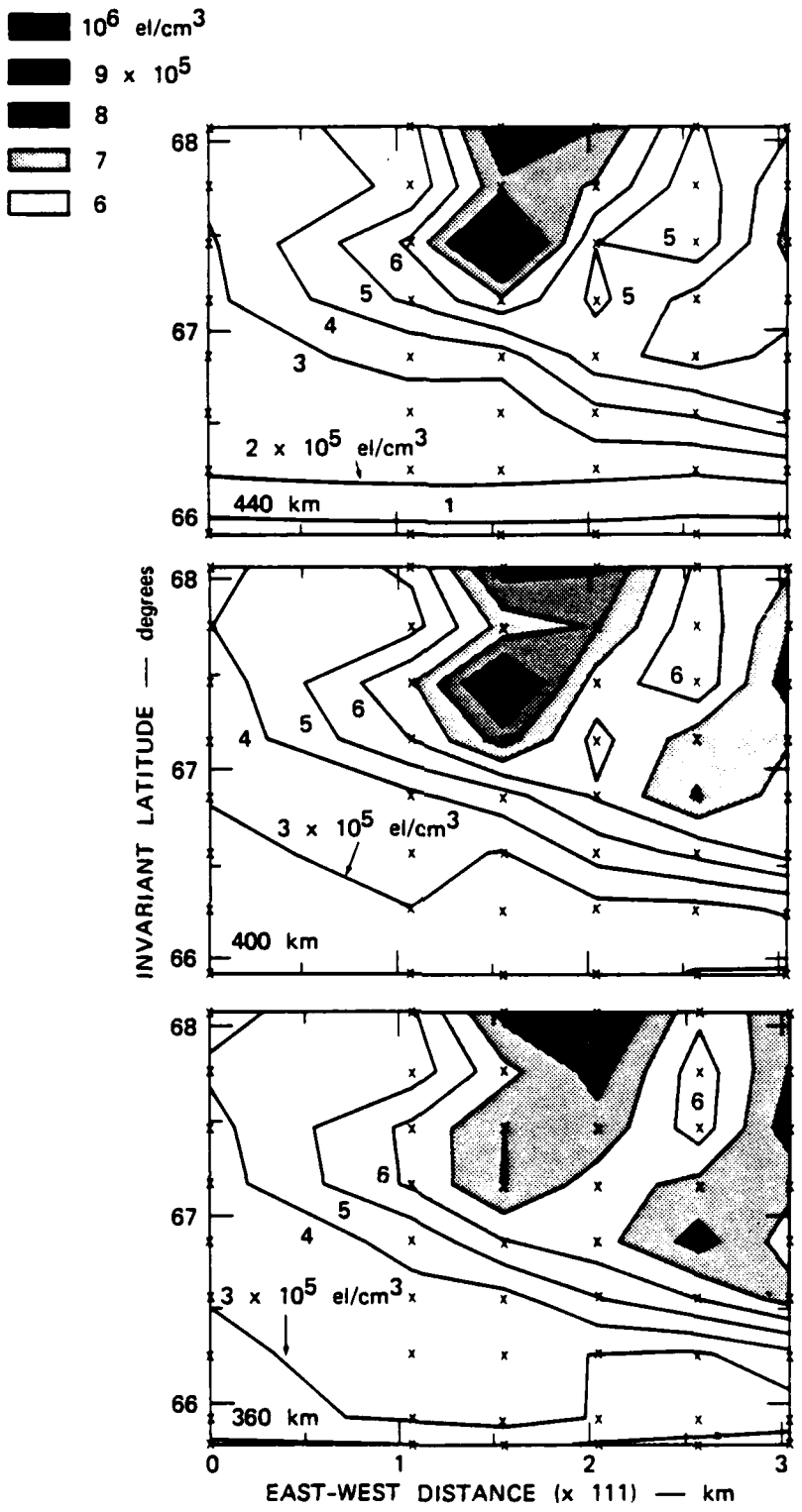

FIGURE 3 CHATANIKA RADAR RECONSTRUCTION OF TRANSVERSE ELECTRON DENSITY PROFILE SHOWING EAST-WEST STRUCTURE

ratio parameters as a:b:1. For sheets, a = b. Wings are intermediate-scale structures with b = a/2.

Figure 4 shows the general pattern established by Livingston et al. (1982). Sheets and wings are confined to the southern region of the scintillation zone. The axial ratio of the rods systematically decreases toward the poleward boundary of the scintillation zone. Wings are generally confined to the near midnight sector. This clearly suggests a close connection with the general pattern of nighttime auroral-zone convection, as shown schematically in Figure 5. These results and their ramifications are discussed in detail in Livingston et al. (1982).

To provide a theoretical framework for interpreting the morphology of scintillation-producing irregularities, the effects of cross-field diffusion in the presence of a conducting E layer have been analyzed (Vickrey and Kelley, 1982). By postulating a source region at the equatorward boundary of the polar cap and a detailed convection model, the lifetime of kilometer-scale irregularities was computed. The details of the model and its ramifications are discussed by Vickrey (1982).

The general features of the model are illustrated in Figure 6, which shows the diffusive decay of a kilometer-scale structure as it convects through the polar cap and into the auroral zone. As discussed by Vickrey (1981), the model reproduces the general features of morphological studies of high-latitude irregularities.

To summarize, we have measured the east-west structure that is predicted theoretically by numerical simulations of the nonlinear evolution of a two-sided, F-region plasma enhancement in the nighttime auroral zone. We have also established a distinct latitudinal and magnetic-local-time variation in the anisotropy of nighttime auroral-zone irregularities. Finally, we are developing a model that contains, at least in rudimentary form, all the essential elements that must be included in a truly predictive (rather than average) high-latitude scintillation model.

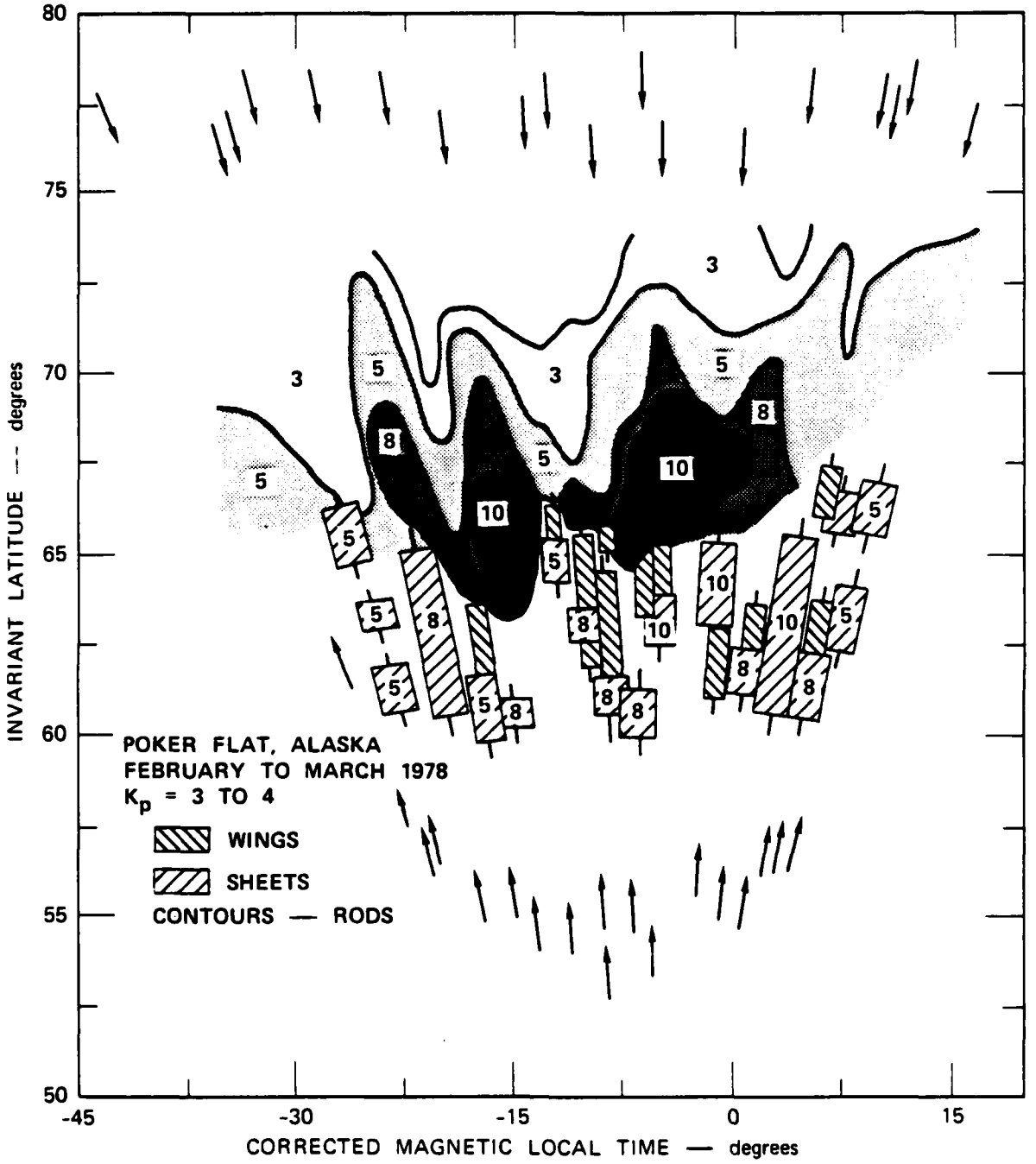

FIGURE 4 MORPHOLOGY OF IRREGULARITY ANISOTROPY UNDER CONDITIONS OF MODERATE ACTIVITY

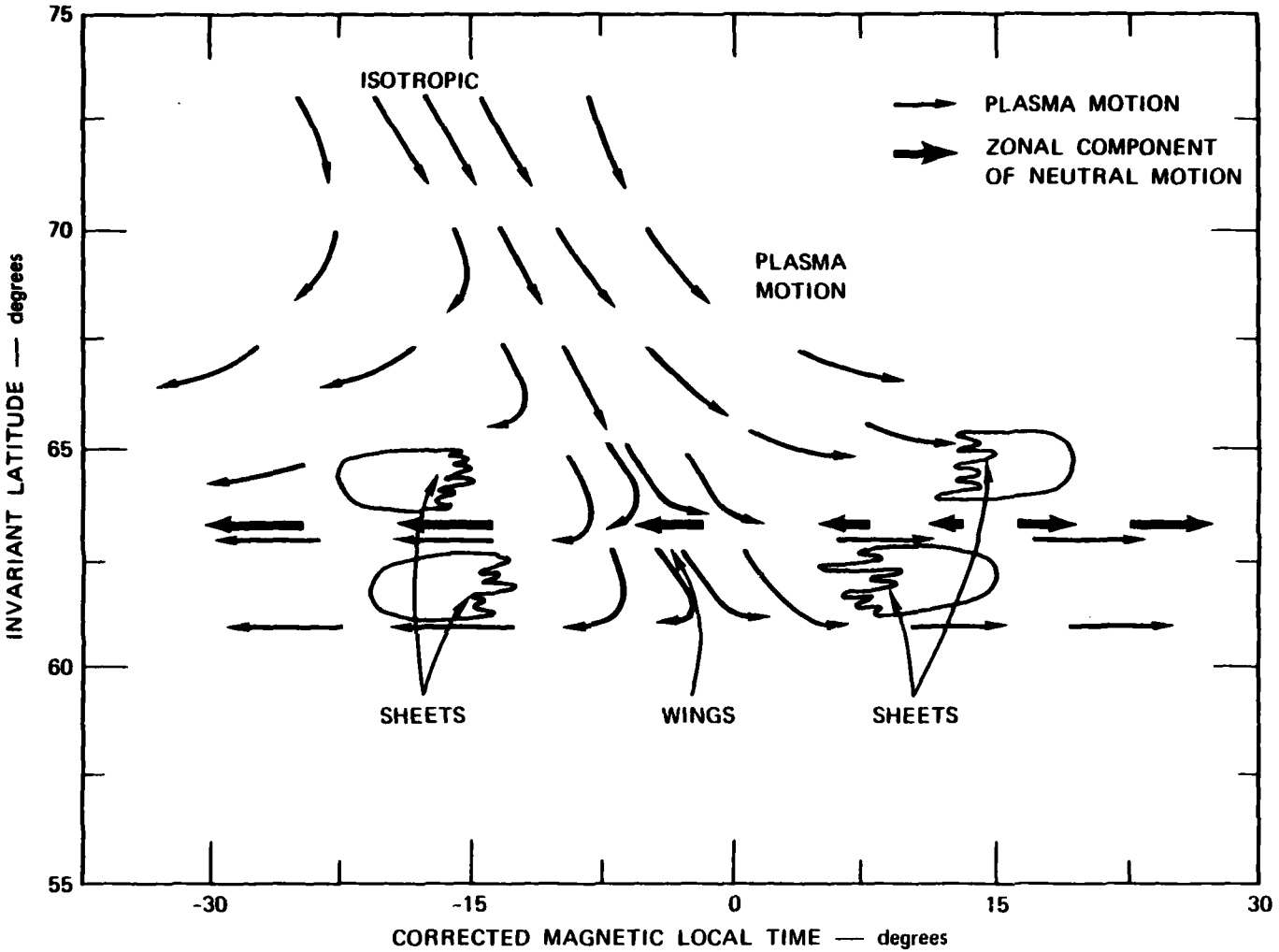

FIGURE 5 SCHEMATIC DIAGRAM OF ANISOTROPY VARIATION AND ITS RELATION TO AVERAGE NIGHTTIME CONVECTION PATTERN

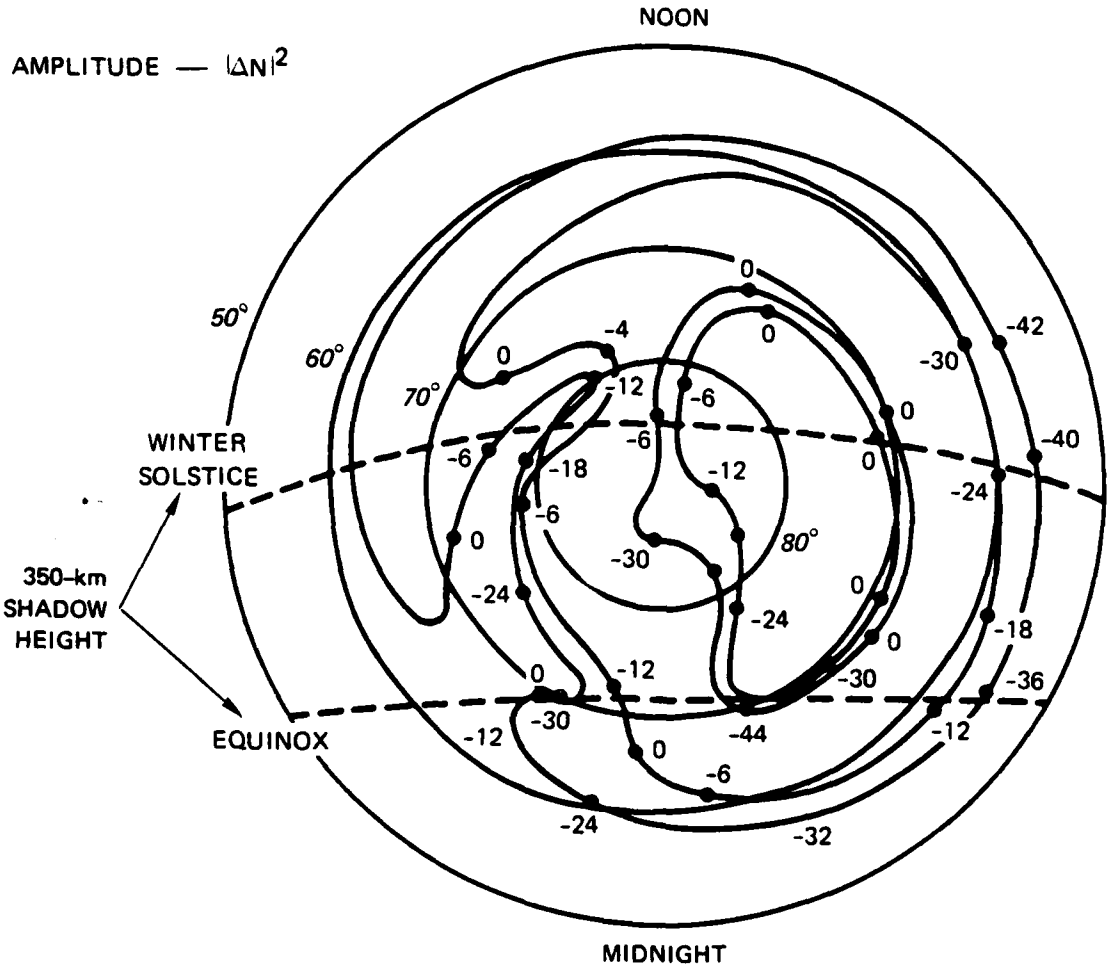

FIGURE 6 MODEL COMPUTATION OF DIFFUSIVE DECAY OF KILOMETER-SCALE IRREGULARITIES

The same considerations apply to the nonlinear evolution of striations that are generated by high-altitude nuclear detonations. In an early-time nuclear environment, of course, conditions are radically different from anything that occurs in the natural ionosphere. The very long lifetimes of F-region plasma structures suggest, however, that the basic features of the model being developed at SRI will ultimately dominate the distribution and configuration of structure. There is much work to be done, and the planned DNA High Latitude satellite will pro-

vide important data for testing the various hypotheses that are used in developing such a model.

III EQUATORIAL STRUCTURE

In 1977 DNA initiated an investigation of plasma-density structure in the nighttime equatorial ionosphere. Interest in equatorial structure, collectively called ESF, was instigated on the hypothesis that the collisional Rayleigh-Taylor instability was the dominant structuring mechanism. This instability is the gravitational analog of the gradient-drift instability, the principal structuring mechanism in the late-time nuclear environment. Investigations of ESF phenomena were conducted from the Kwajalein Atoll, Marshall Islands, in field experiments during each of five summers, 1977 through 1981, including a highly successful rocket (Plumex I) campaign in 1979.

In the following subsections, we summarize the experimental results obtained from this series of field programs and discuss what we consider to be the remaining major questions. The results are divided into four categories, according to irregularity scale size: large, intermediate, transitional, and small.

A. Large-Scale Structure (Greater than 10 km)

Investigations of ESF irregularities have shown that the structuring process is initiated at large scales (i.e., greater than 10 km) and proceeds through an apparent hierarchy of plasma instability processes that produce smaller scales (e.g., Haerendel, 1973). The structuring mechanism acting at these largest scales appears to be the collisional Rayleigh-Taylor instability. During the early stages of theoretical development, the collisional Rayleigh-Taylor instability was proposed as a possible mechanism (Dungey, 1956). However, the theory was played down because irregularity growth appeared to be possible only in the bottomside F layer, whereas ESF also occurred in the topside F layer (e.g., Farley et al., 1970). Scannapieco and Ossakow (1976) have since shown that the nonlinear collisional Rayleigh-Taylor instability could

account for irregularities found both in the bottomside and topside of the F layer.

The Kwajalein experimental results have shown conclusively that the nonlinear numerical simulations of the collisional Rayleigh-Taylor instability (Scannapieco and Ossakow, 1976; Ossakow et al., 1979; Zalesak and Ossakow, 1980) correctly describe the development of large-scale plasma depletions, or bubbles. The procedure for experimental verification was as follows. First, radar backscatter plumes, observed with the ALTAIR radar (Tsunoda et al., 1979) were shown to be collocated with plasma bubbles (Tsunoda and Towle, 1979; Tsunoda, 1980a,b; Towle, 1980; Szuszczewicz et al., 1980). The temporal evolution of plasma bubbles could then be followed by examining a time sequence of spatial maps of ESF backscatter obtained with ALTAIR, a steerable radar.

Primary structuring of large-scale irregularities began in the bottomside F layer in the form of upwellings (Tsunoda, 1981; Tsunoda and White, 1981). Examples of bottomside upwellings can be seen in Figure 7. Three upwellings appear in the figure as altitude modulations in the isodensity contours. The upwellings then push upward, forming plasma bubbles, and penetrate into the topside F layer. The upward development of plasma bubbles, mapped spatially as radar backscatter plumes, is illustrated in Figure 8. The growth of plasma bubbles into vertically elongated "wedges" was similar to the numerical simulations of the collisional Rayleigh-Taylor instability by comparing the spatial relationship of backscatter plumes to plasma depletions measured in situ in the neck region of plumes by the Atmospheric Explorer E satellite (Tsunoda et al., 1982).

The description of large-scale structure (i.e., plasma bubbles) as a two-dimensional process appears justified provided that the description uses flux-tube-integrated quantities (Haerendel, 1973; Anderson and Haerendel, 1979). The field-aligned nature of plasma bubbles was substantiated with ALTAIR by mapping a plasma bubble (using incoherent-scatter measurements) over more than ten degrees of magnetic dip latitude (Tsunoda, 1980b). A map of a plasma bubble in altitude and magnetic-dip latitude is shown in Figure 9.

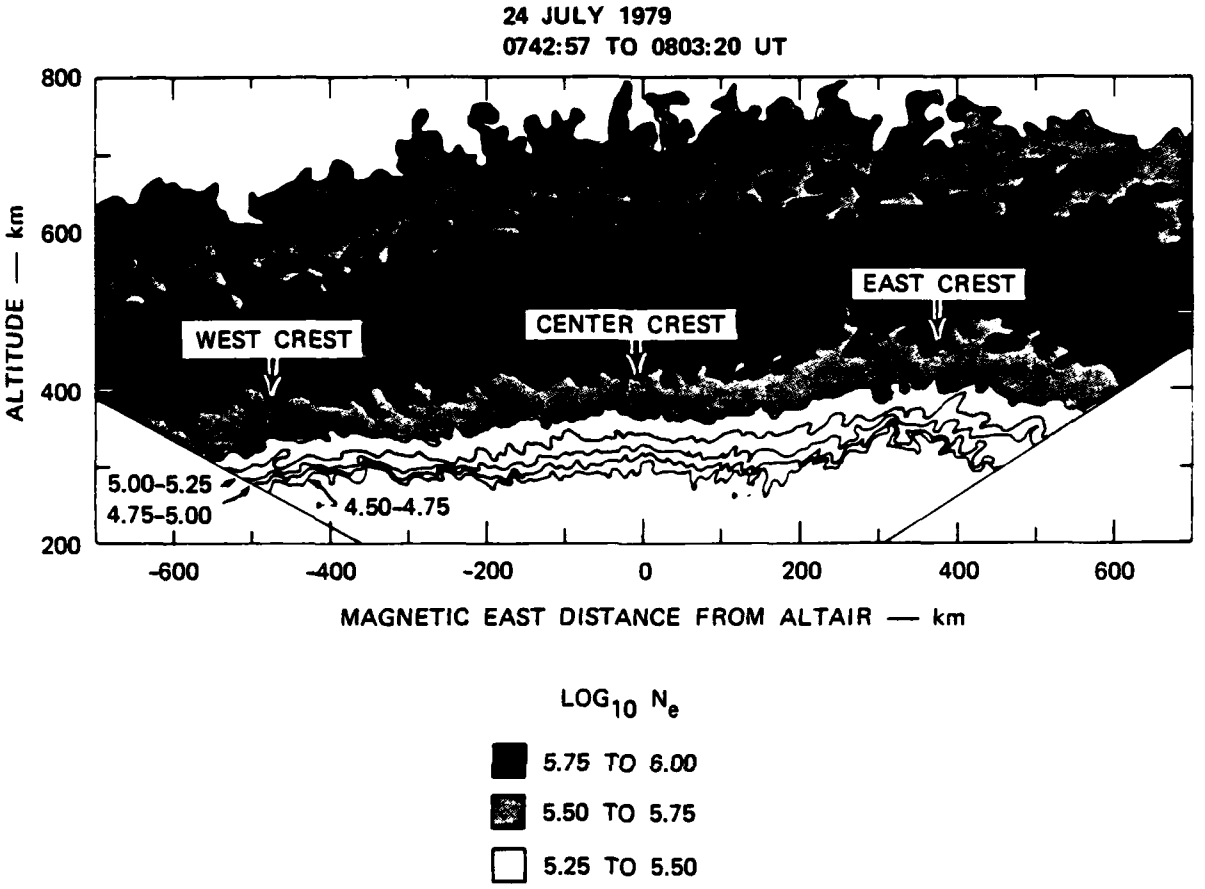

FIGURE 7 EVIDENCE OF WAVE STRUCTURE IN CONTOURS OF CONSTANT ELECTRON DENSITY FOUND IN THE BOTTOMSIDE F LAYER BEFORE THE DEVELOPMENT OF ESF BACKSCATTER

In addition to the primary structuring, ALTAIR results indicated that secondary structuring occurred regularly along the western walls of bottomside F-layer upwellings (Tsunoda, 1981; Tsunoda and White, 1981). Tsunoda (1981) suggested that this secondary structuring was produced by the gradient-drift instability driven by an eastward neutral wind blowing through the western walls of upwellings. In Figure 10, the structuring of the western wall of an upwelling is illustrated. By

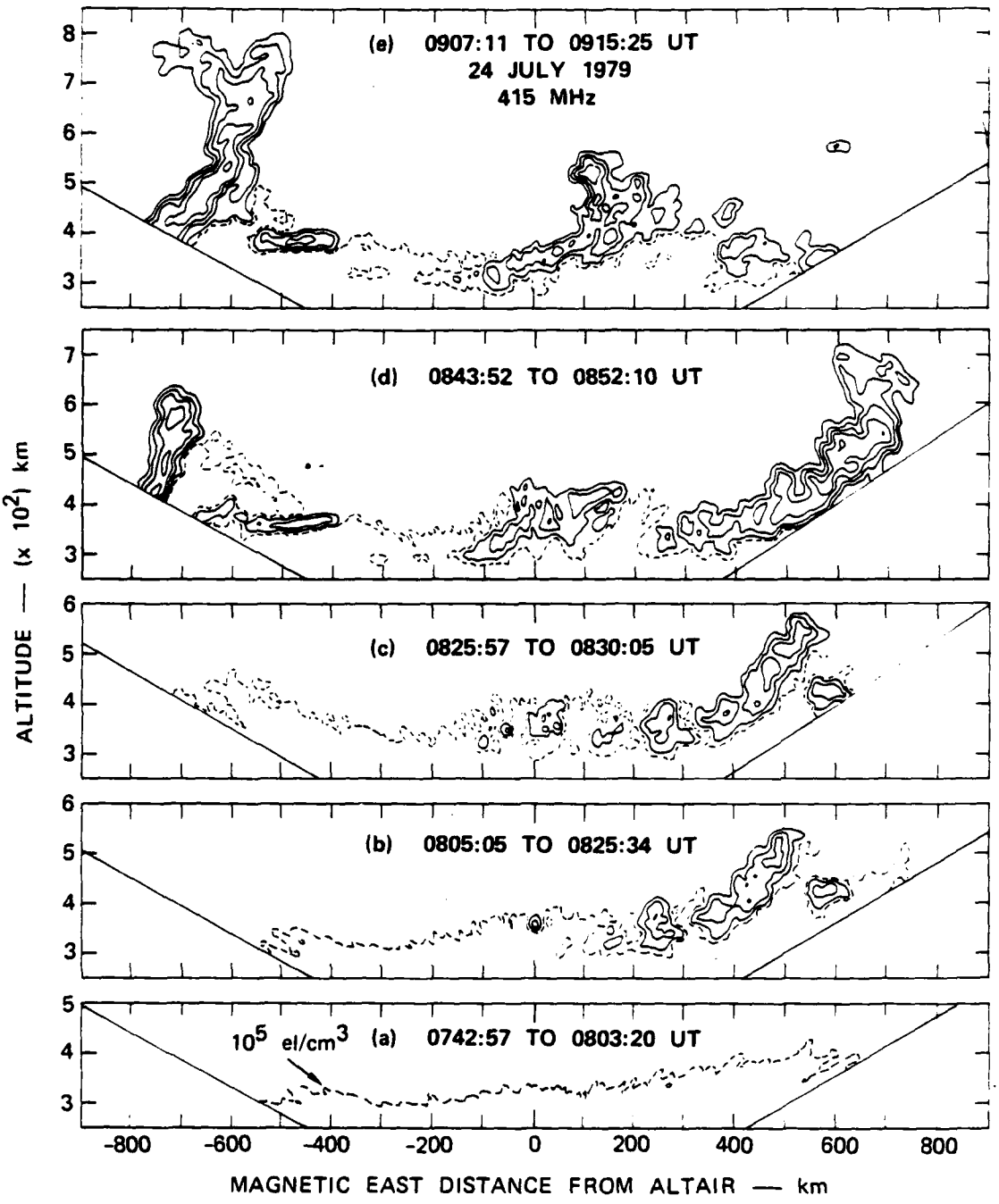

FIGURE 8 SEQUENCE OF ALTAIR BACKSCATTER MAPS SHOWING THREE UPWELLINGS THAT DEVELOP ESF BACKSCATTER ALONG THEIR WEST WALLS, FOLLOWED BY PLUME DEVELOPMENT

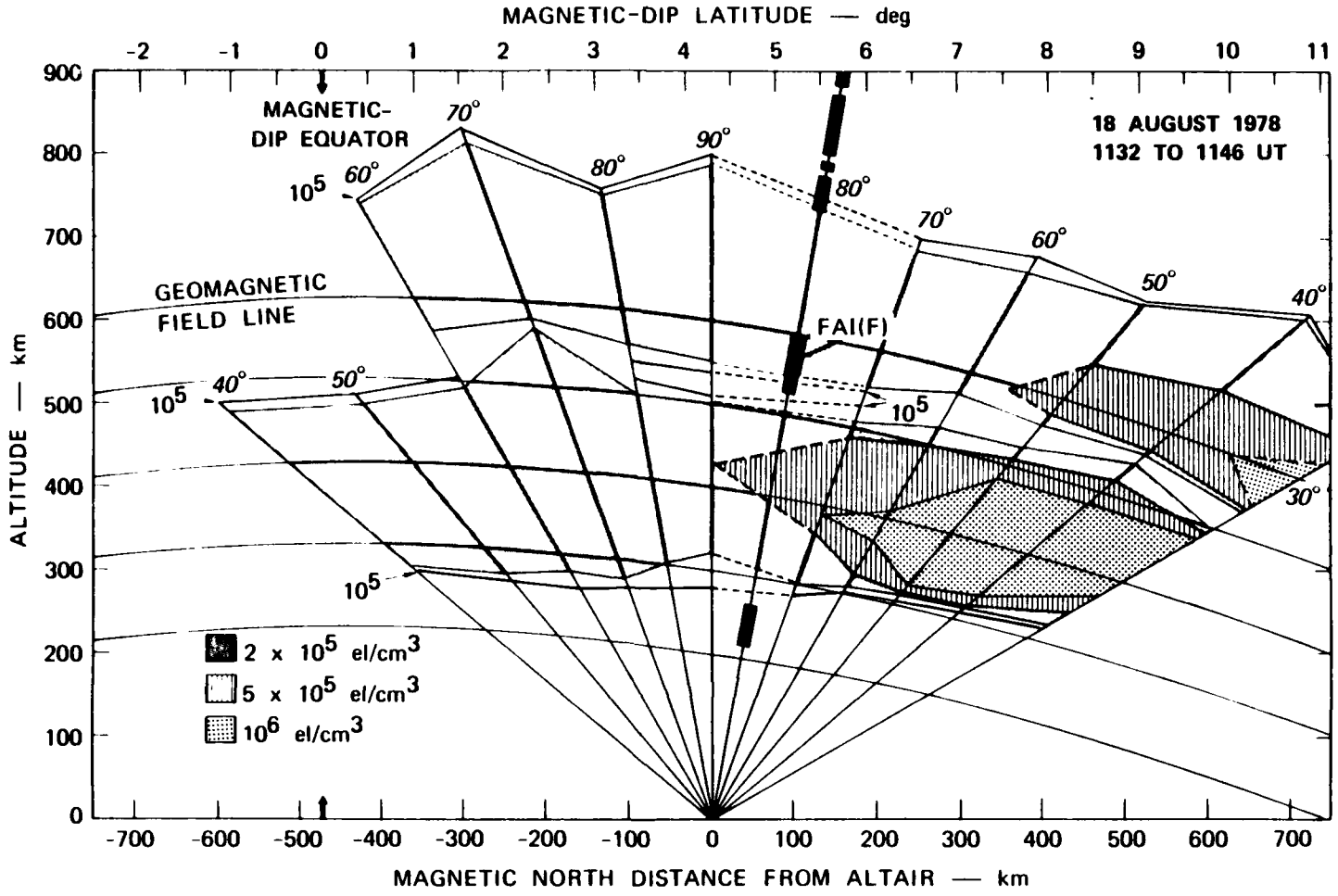

FIGURE 9 CONTOUR MAP SHOWING THE LATITUDINAL DISTRIBUTION OF ELECTRON DENSITY GREATER THAN 2 X 10^5 el/cm^3 (SHADED REGIONS) AND THE MAGNETIC-FIELD ALIGNMENT OF THE PLASMA DEPLETION (GAP BETWEEN THE SHADED REGIONS)

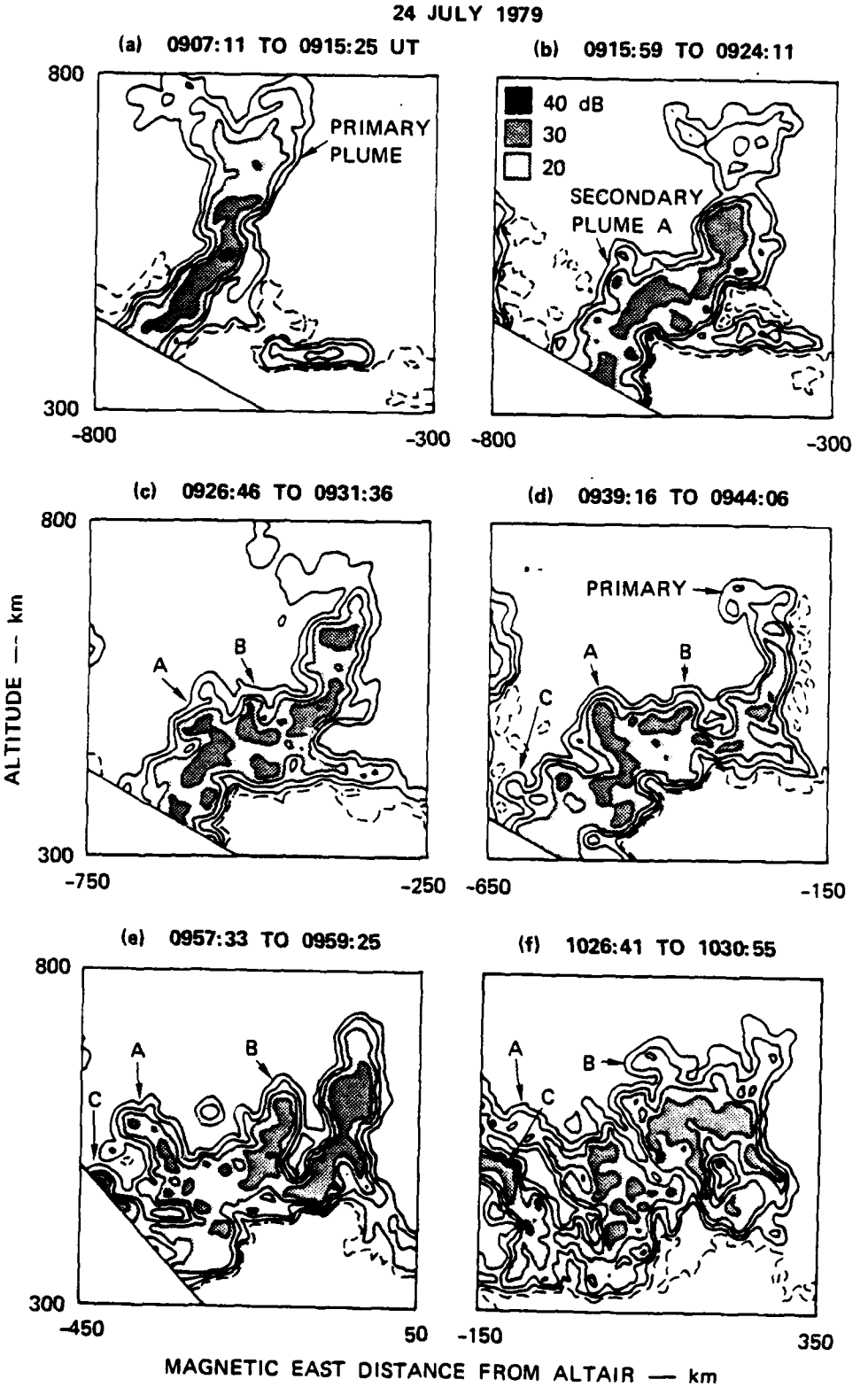

FIGURE 10 SEQUENCE OF ALTAIR BACKSCATTER MAPS THAT SHOW THE STRUCTURING OF THE WEST WALL OF AN UPWELLING

tracking the plume seen in the upper left hand corner of Figure 8, we find that the western wall continues to structure over a period of more than an hour, even after the decay of the primary plume. The structuring appears in the form of smaller-scale plasma bubbles or irregularities. The strong backscatter from the western wall and the absence of backscatter from the eastern wall strongly supports the proposed gradient-drift mechanism. (We should note, of course, that because the upwelling is located in the bottomside F layer, the collisional Rayleigh-Taylor instability is also operative there.) Szuszczewicz et al. (1981) showed that the Plumex II rocket measurements (launched 0957:30 UT) found relatively weak plasma-density structure within the eastern wall of the upwelling in Figure 10(e).

Conclusive evidence for the action of the gradient-drift instability along the western wall of the upwelling is presented in Figure 11. The east-west plasma drift was estimated by measuring the horizontal displacements of traceable backscatter features in Figure 8. Tsunoda et al. (1981) showed that the east-west plasma drift is characterized by a velocity shear with altitude. The velocity shear is evident in Figure 11 by noting that the solid bars correspond to high-altitude measurements and the dashed bars correspond to low-altitude measurements. The velocity difference exceeds 100 m/s. Figure 11 also shows the eastward neutral wind, measured simultaneously with a Fabry-Perot interferometer (Sipler et al., 1980). Fabry-Perot interferometer measurements refer to the bottomside of the F layer in which 630.0-nm emissions are most intense. The neutral wind is seen to accelerate, starting around 0745 UT, and approach the mean eastward plasma drift at high altitudes. The ion-neutral slip velocity that drives the gradient-drift instability is the difference between the low-altitude plasma drift (dashed bars) and the neutral wind. From this figure, there is little doubt that the western wall was structured primarily by the gradient-drift instability. Figure 12 summarizes the experimental results on large-scale ESF structure, published to date. Structuring appears to be initiated by an upwelling in the bottomside F layer [Figure 12(a)]. The upwelling pushes upwards [Figure 12(b)] via the collisional Rayleigh-Taylor instability,

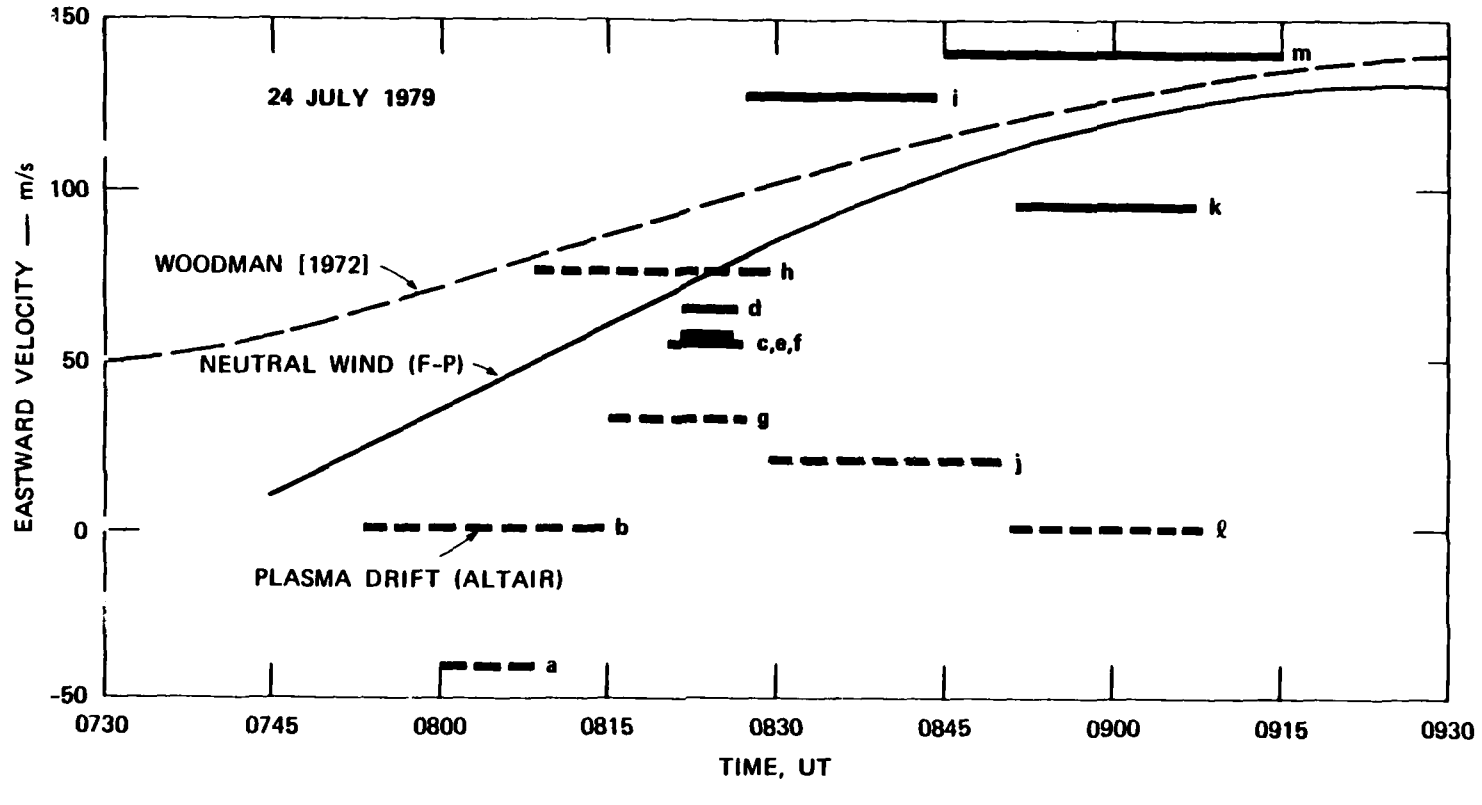

FIGURE 11 SIMULTANEOUS MEASUREMENTS OF F-REGION PLASMA DRIFT (SOLID AND DASHED BARS) AND NEUTRAL WIND (SOLID CURVE), REVEALING A SIGNIFICANT SLIP VELOCITY AT LOW ALTITUDES

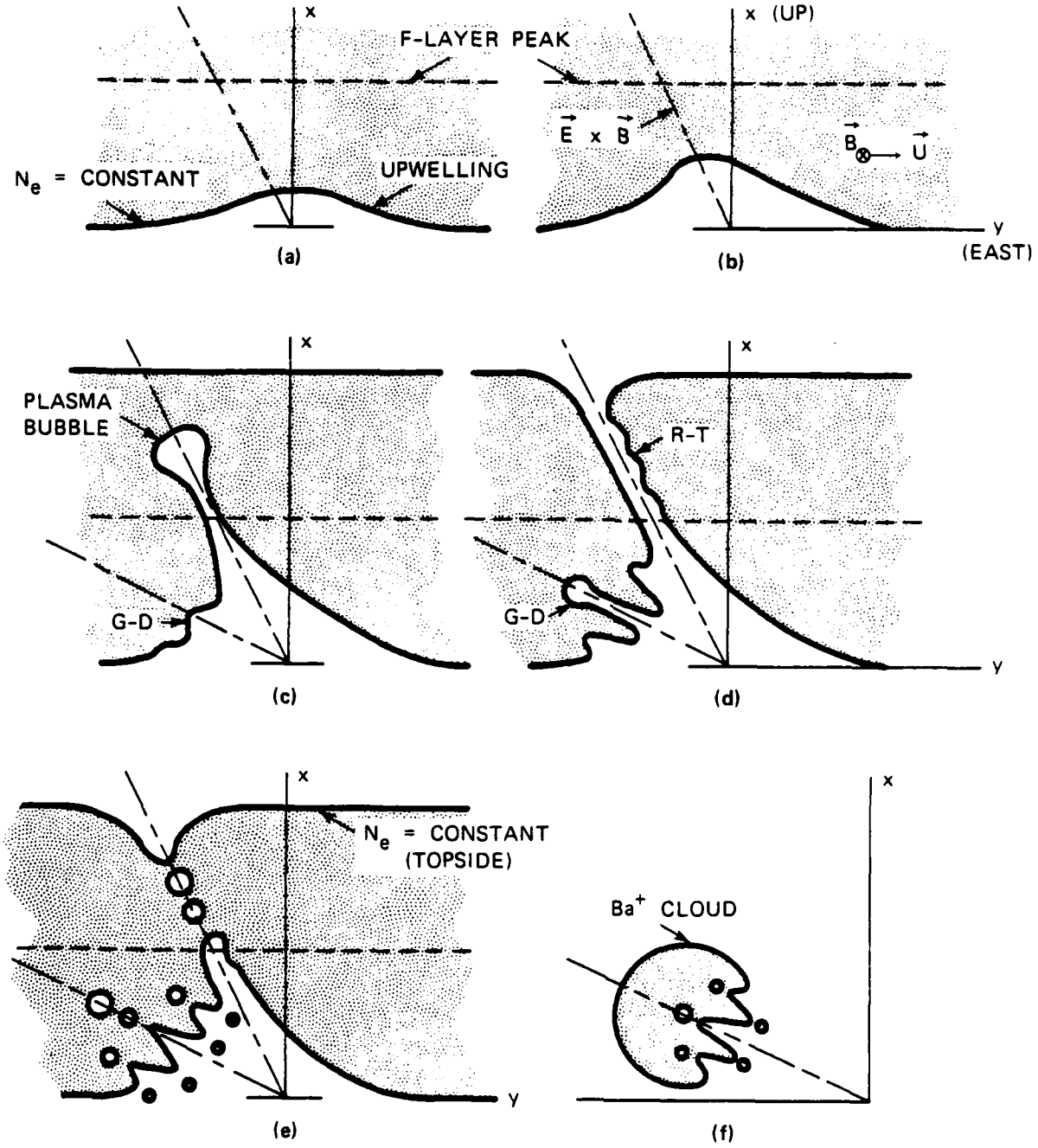

FIGURE 12 DESCRIPTIVE MODEL OF PLASMA STRUCTURING IN THE EQUATORIAL F LAYER PRODUCED BY THE GRADIENT-DRIFT AND COLLISIONAL RAYLEIGH-TAYLOR INSTABILITIES

producing a plasma bubble that penetrates into the topside F layer [Figure 12(c)]. The bubble continues to develop upward until it reaches an altitude at which the ambient plasma density is identical to that within the bubble [Figure 12(d)]. Structuring of the eastern wall of the wedge (formed by the upward-developing plasma bubble) at high altitudes might occur via the Rayleigh-Taylor instability, which, together with cross-field diffusion, could then act to close the wedge [Figure 12(e)]. At the same time, the western wall of the upwelling (in the bottomside F layer) begins to structure via the gradient-drift instability, driven by an eastward neutral wind [Figures 12(d) and 12(e)]. The slip velocity is enhanced in the upwelling by a velocity shear that is produced by the F-region dynamo acting in the presence of an altitude-dependent Pedersen conductivity. The analogy of the western wall of the upwelling to the well-known structuring of a barium ion cloud is illustrated in Figure 12(f).

More recent (and as yet unpublished) results of ALTAIR data analysis indicate that the scenario depicted in Figure 12 is not the only process by which plasma bubbles and backscatter plumes develop. Figure 13 illustrates another scenario. The sequence of contour maps constructed from ALTAIR backscatter data taken on 22 July 1979 reveals bubble and plume development without the presence of a large-scale upwelling. In Figure 13(a), we see the occurrence of a wedge or bubble in the bottomside F layer with backscatter associated with its upper wall. There is no evidence of any large-scale wave structure in the bottomside plasma-density contour, as reported by Tsunoda and White (1981). [For example, compare Figure 13(a) to Figure 7 or 8(a)].

In the next three maps [Figures 13(c) to 13(e)], we observe a slight clockwise rotation of the plume as it continues to develop upward. Moreover, a "kink" develops in the neck of the plume [Figure 13(d)]. Both the kink and the clockwise rotation can be explained in terms of a velocity shear. The plasma-density profile taken along the radial line to the right of the plume in Figure 13(e), is shown in Figure 14. We find that the peak of the F layer occurred around the 530-km altitude and the steep bottomside gradient occurred below about

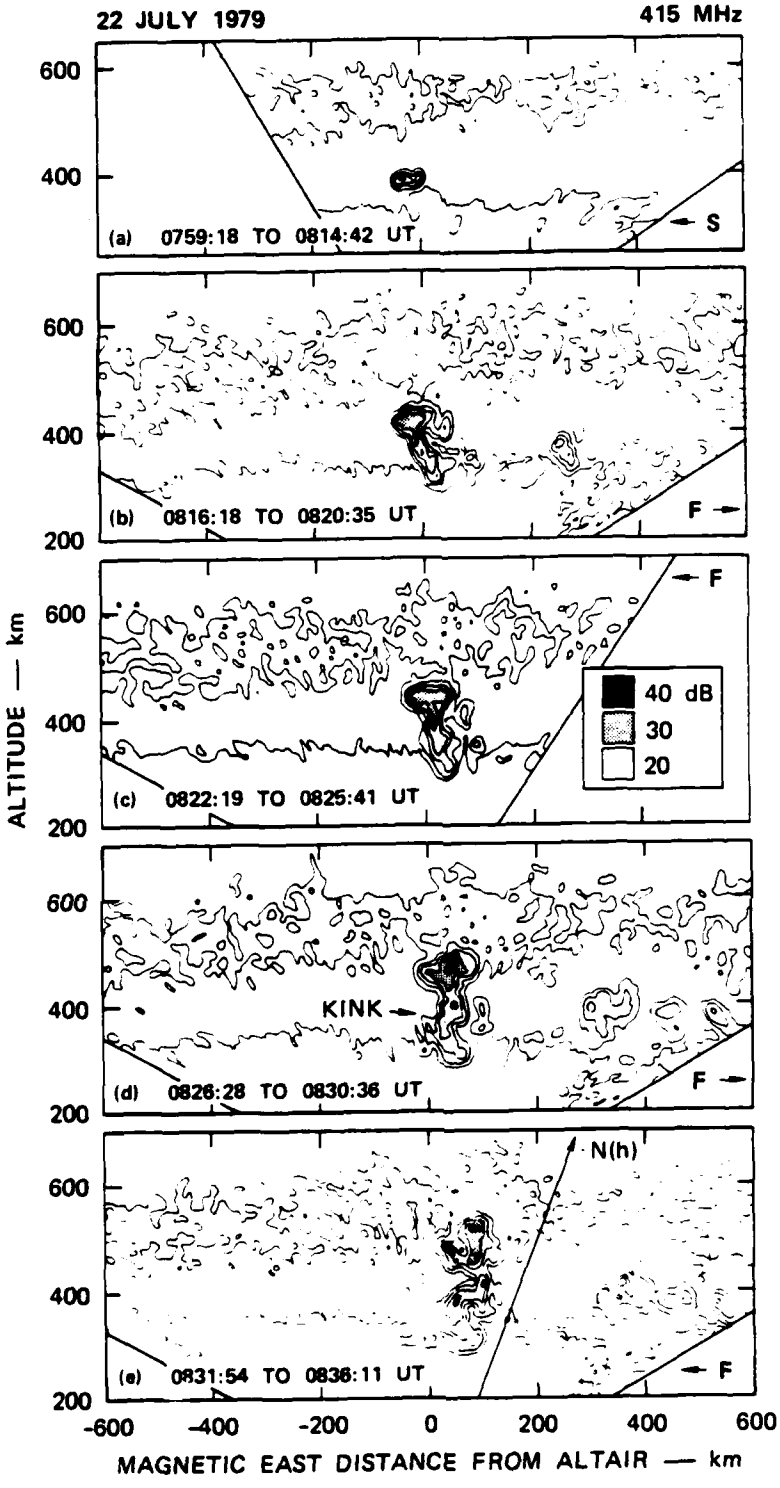

FIGURE 13 SEQUENCE OF ALTAIR BACKSCATTER MAPS SHOWING THE DEVELOPMENT OF ESF PLUMES WITHOUT LARGE-SCALE UPWELLINGS IN THE BOTTOMSIDE F LAYER AND THE DISTORTION OF THOSE PLUMES BY VELOCITY SHEAR

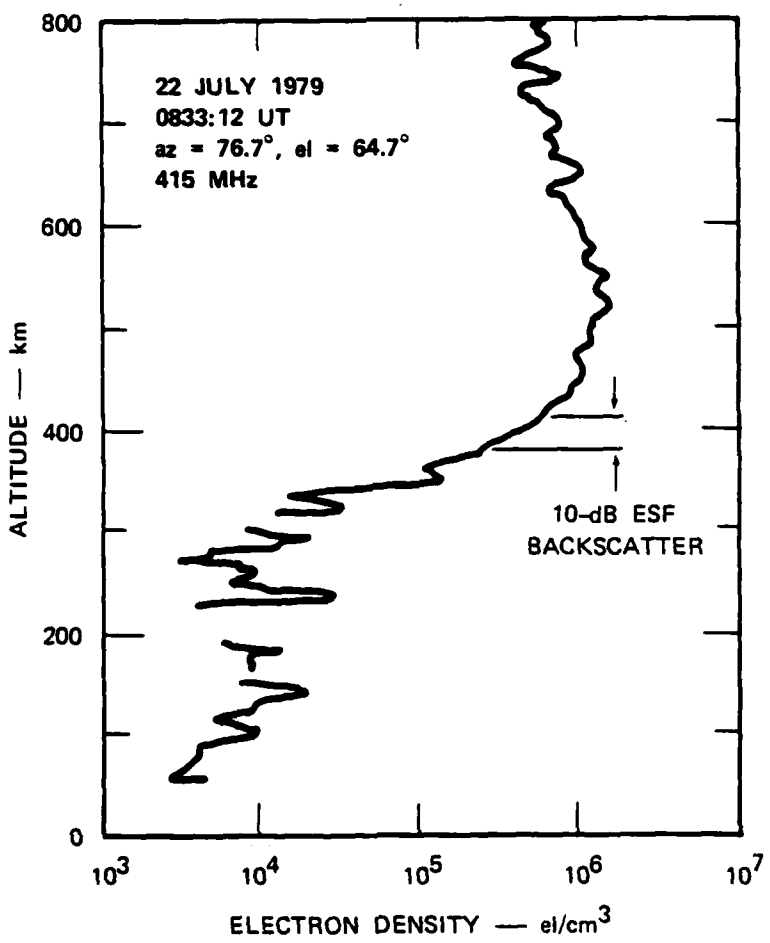

FIGURE 14 ELECTRON-DENSITY PROFILE OBTAINED ALONG RADIAL LINE IN FIGURE 13(e)

400 km. The clockwise rotation of the plume, therefore, appears to be associated with the slowly varying portion of the plasma-density profile and the kink with the steep bottomside profile. This interpretation is consistent with the numerical simulations of Rayleigh-Taylor bubbles by Zalesak et al. (1982). In their simulation, they showed that in the presence of finitely conducting E layer, the velocity shear is directly related to the F-layer Pedersen conductivity profile.

A similar plume development sequence is seen in the contour maps presented in Figure 15. In these maps, which follow immediately after

the last map in Figure 13, we see that appearance of another wedge [Figure 15(a)], followed by its development into a small plume in Figures 15(c) to 15(e). Similar velocity shear effects are also present. It is interesting to note that in spite of the initial absence of large-scale wave structure and upwellings in the bottomside F layer, the plumes are still spaced a few hundred kilometers apart; in this case, 350 km. There is also evidence in Figure 15 that a large-scale wave structure (upwellings) appears to develop in Figures 15(c) to 15(e), after the development of at least two of the plumes. The plume near the left side of all the maps in Figure 15, however, might have been generated after the development of upwellings.

The above-described results indicate that large-scale wave structure does not have to be present to initiate the generation of bubbles and plumes. Yet Tsunoda and White (1981) showed that the collisional Rayleigh-Taylor instability does not appear to be capable of amplifying thermal fluctuations to detectable levels, and that a seed perturbation appears necessary.

The question as to what controls bubble or plume development remains. This question is analogous to what controls the bifurcation tendency of barium (or nuclear-produced) plasma clouds. In the case of the initial formation of bubbles, we are dealing with a slab-like geometry, although upwellings provide a more concave surface. In the case of bifurcation of plasma bubbles or plumes, we are dealing with a much smaller radius of curvature.

An example of plume (and bubble) bifurcation can be seen in the plume in Figure 10(a). There is a distinct indentation in the head of the plume, apparently forming two separate secondary bubbles. All plumes, however, do not bifurcate to the same extent. An example is the left plume in Figure 15(e). A later map of the same plume is presented in Figure 16. There is no obvious bifurcation. Finally, we present an outstanding example of extensive plume bifurcation in Figure 17. This plume, observed on 10 July 1980, displays a two-step bifurcation history. Apparently, the primary bubble (plume) first trifurcated to form secondary bubbles labeled 1, 2, and 3. Secondary bubble 1 then trifurcated to form tertiary bubbles labeled a, b, and c.

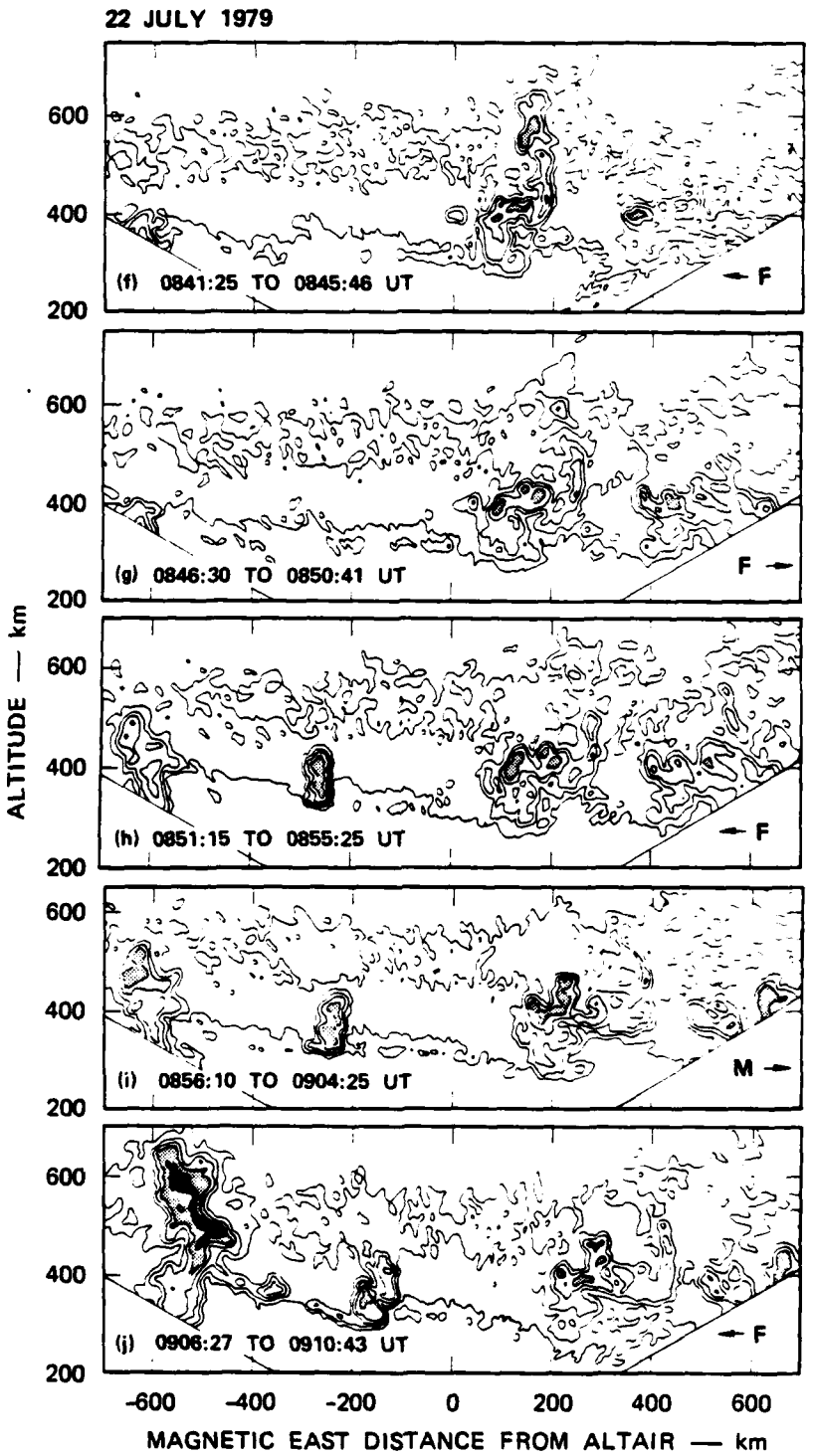

FIGURE 15 CONTINUATION OF THE SEQUENCE OF ALTAIR BACKSCATTER MAPS SHOWN IN FIGURE 13

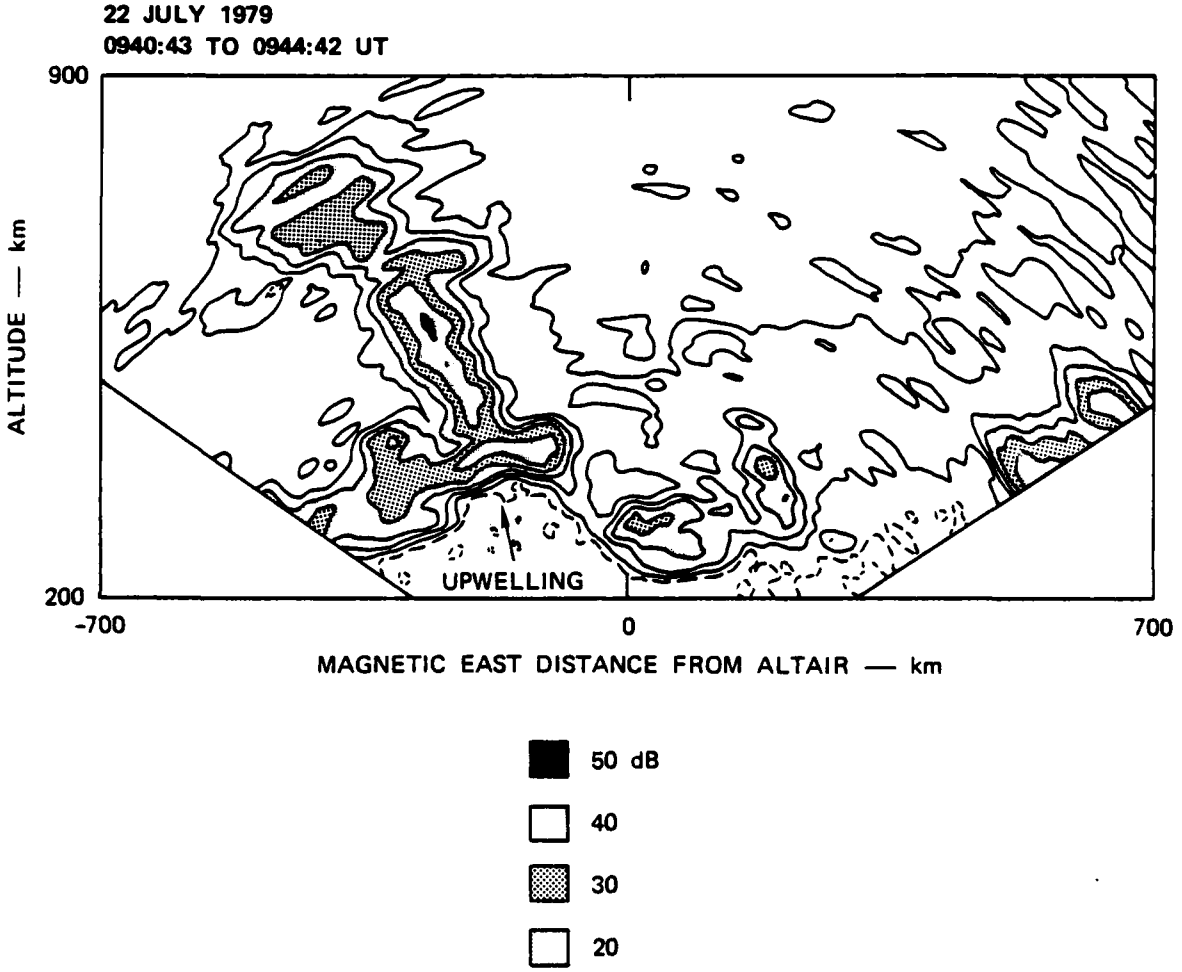

FIGURE 16 EXAMPLE OF AN ESF BACKSCATTER PLUME THAT HAS DEVELOPED WITHOUT ANY BIFURCATION

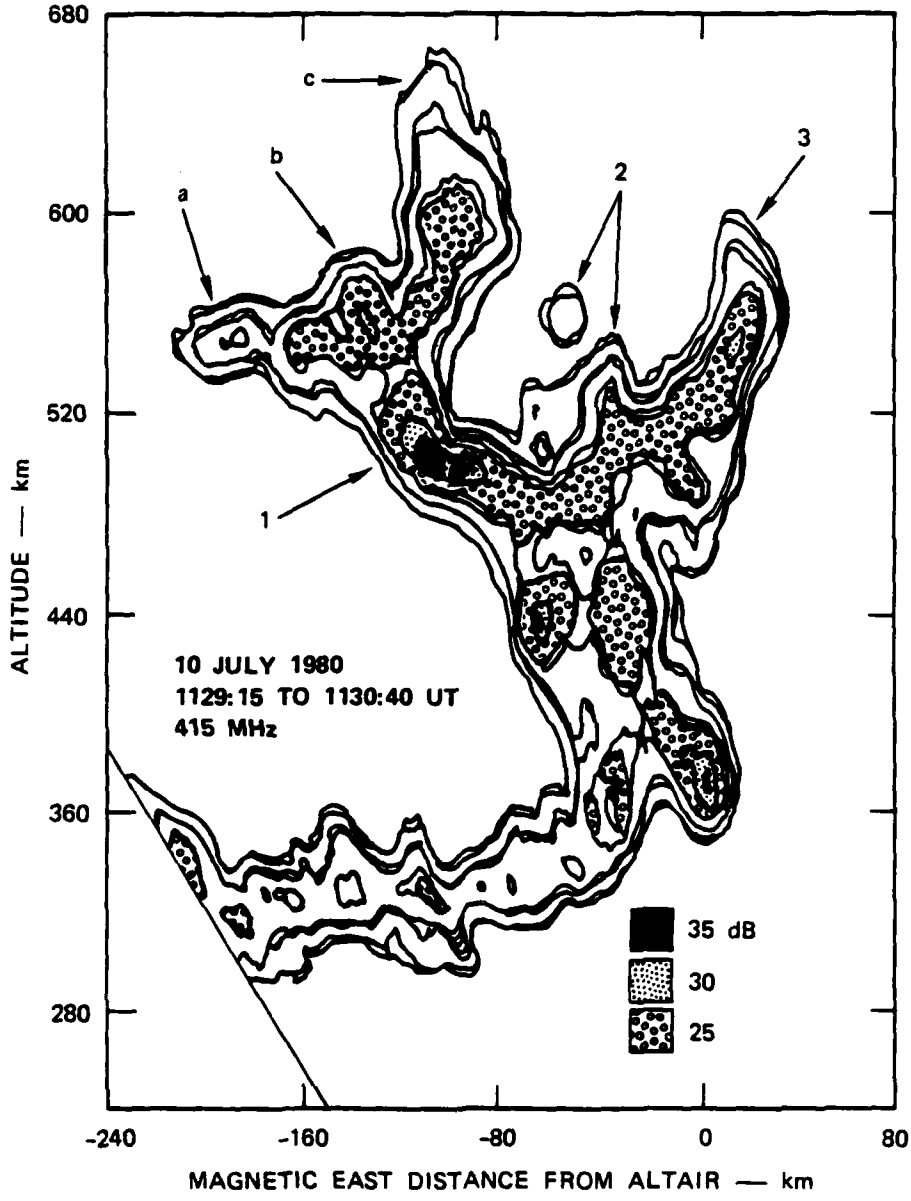

FIGURE 17 ALTAIR BACKSCATTER MAP SHOWING PROGRESSIVE STRUCTURING OF BACK-SCATTER PLUME

B. Intermediate-Scale Structure (10 km to 100 m)

The spatial wavelengths labeled as intermediate scale structure include the short end of the irregularity spectrum believed to be produced by the collisional Rayleigh-Taylor instability. At a 100-m spatial wavelength, finite gyroradius effects are still minimal, particularly in a collisional plasma (Hudson and Kennel, 1975). At shorter wavelengths (transitional and small-scale structure), other plasma processes begin to dominate the production of structure.

Our understanding of intermediate-scale structure has been advanced by scintillation measurements and by in situ satellite and rocket measurements. Scintillation measurements were made at Kwajalein by using the polar-orbiting Wideband satellite and the Plumex I rocket. In situ measurements also were made by the Plumex I rocket.

Phase-scintillation measurements using the Plumex I rocket beacon contain evidence that the principal scintillation-producing irregularities are imbedded in high plasma-density regions adjacent to plasma bubbles (Rino et al., 1981). Strong scintillations were not associated with plasma-depleted regions. This conclusion, however, requires further verification because the plasma bubble probed by the Plumex I rocket was decaying. It is possible that intermediate-scale structure is associated also with plasma-depleted regions during the growth phase of plasma bubbles.

Perhaps a more significant finding, from in situ rocket and scintillation measurements, was that the spectral slope associated with intermediate-scale structure depends on the strength of the irregularities (Livingston et al., 1981; Rino et al., 1981). Both Wideband and rocket beacon-scintillation measurements and in situ AE-E satellite measurements contain evidence that the slope tended to become more shallow with increasing turbulence strength. As yet, there is no satisfactory explanation for the slope dependence on turbulence strength.

In addition to depending on turbulence strength, the spatial irregularity spectrum measured by the Plumex I rocket was best represented by two spectral slopes, with the breakpoint located around 500 m (Rino et al., 1981). An example of the irregularity spectrum obtained during the rocket upleg at the 316-km altitude is shown in Figure 18. This dual slope characteristic appeared confined to lower altitudes at which the largest perturbations developed as shown in Figure 19. The spectral slopes have been plotted as a function of altitude. The two spectral indices converge towards a value near two at an altitude between 350 and 400 km. Rino et al. (1981) suggested that the spatial wavelength of 500 m might be a manifestation of the stirring scale length associated with two-dimensional plasma turbulence, e.g., in the scenario proposed by Kelley and Ott (1978).

An alternate explanation for variations in spectral slope would be the presence of more than a single driver. If the outer scale of the irregularity spectrum is determined by the initial gradient scale length (Keskinen et al., 1980), two drivers might be acting on different initial gradient scale lengths to produce a composite spectrum that is characterized by two spectral slopes. Tsunoda (1981) proposed that, in addition to the collisional Rayleigh-Taylor instability, the gradient-drift instability was probably operative. With the gradient-drift instability acting on the western wall of large-scale upwellings (see Section III-A), driven by an eastward neutral wind, we might expect an input gradient scale length associated with the western wall or with primary irregularities. Because the velocity shear that allows the gradient-drift instability to be operative is present only in the bottomside F layer, it is tempting to associate the altitude dependence seen in Figure 19 with a dual driver mechanism. This concept, however, still remains to be clarified.

C. Transitional-Scale Structure (100 m to 10 m)

The transitional-scale regime represents that portion of the spatial irregularity spectrum that is produced by decreasing contributions by the collisional Rayleigh-Taylor instability, and increasing contribu-

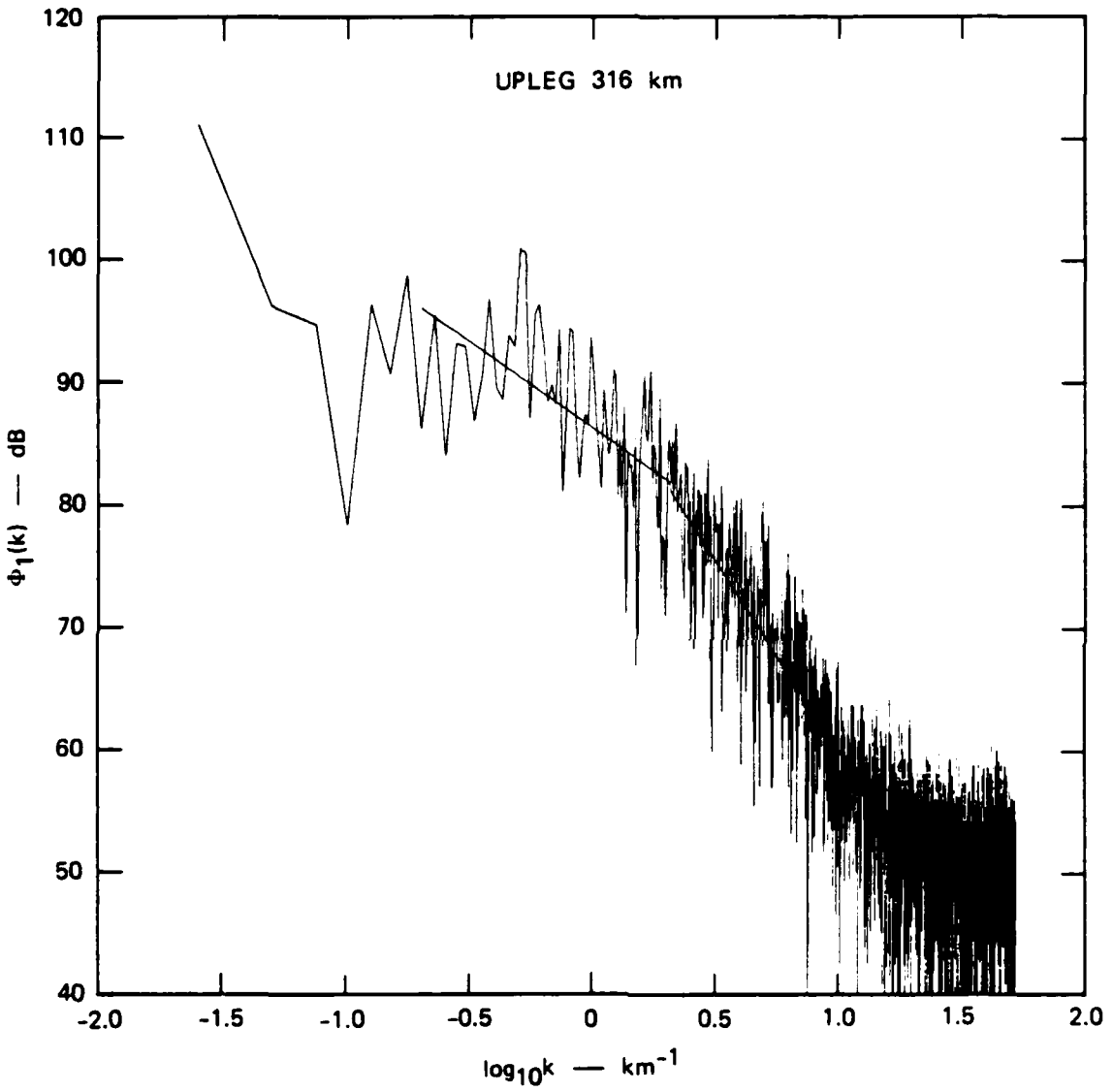

FIGURE 18 ESF IN SITU SPECTRAL DENSITY FUNCTION MEASURED DURING DNA PLUMEX EXPERIMENT CAMPAIGN

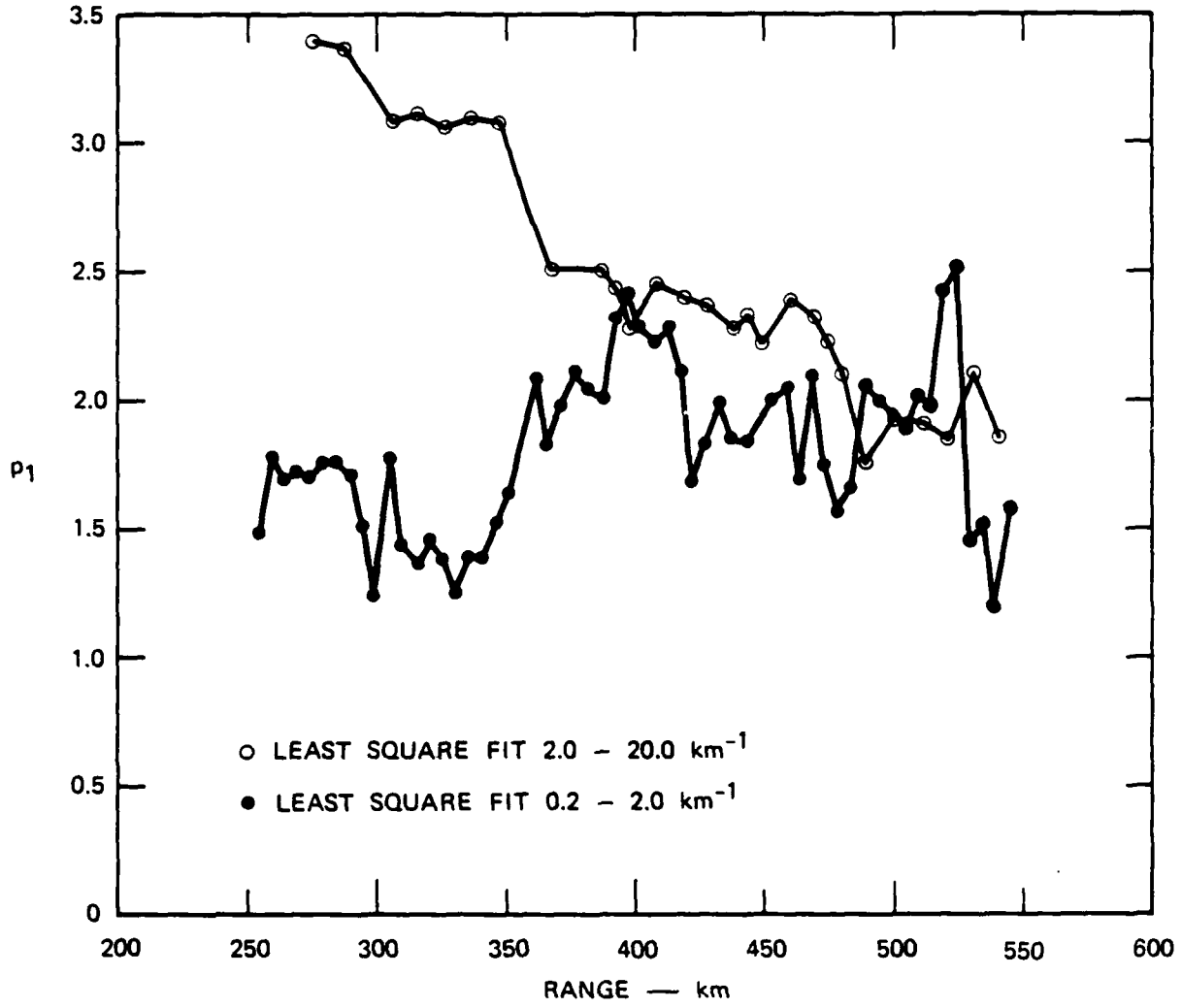

FIGURE 19 MEASUREMENTS OF POWER-LAW INDEX IN LARGE-SCALE AND SMALL-SCALE SPECTRAL REGIMES FROM DNA PLUMEX ROCKET CAMPAIGN

tions by other plasma processes. The collisional Rayleigh-Taylor instability is damped at these wavelengths by finite gyroradius effects. Other plasma processes include excitation of drift waves and diffusion. Drift-wave instabilities are presumably driven by the gradients associated with larger-scale irregularities produced by the collisional Rayleigh-Taylor instability. It is not yet clear whether linear excitation of drift waves occurs or whether turbulent cascade occurs through wave-wave coupling.

Structure at these wavelengths was measured in situ by plasma probes on the Plumex I rocket. These structures correlated with the intermediate-scale structure. This correlation is consistent with the concept that low-frequency drift waves are driven by the larger-scale irregularities.

Kelley et al. (1982) showed that the low-altitude spectrum differed from the high-altitude spectrum in that the former could be expressed with two spectral slopes whereas the latter was best described with a single spectral slope. The spectral slope varied from -2 to -5 with a changeover occurring around an irregularity wavelength of 22 m. The high-altitude spectrum was characterized by a spectral slope of -5. Kelley et al. (1982) thought that the -5 slope was consistent with drift waves and that the crossover wavelength was the ion gyroradius. The confinement of the two-slope spectrum to low altitudes was interpreted in terms of an altitude threshold for drift-wave turbulence. That is, anomalous diffusion was assumed operative above the 280-km altitude, and collisional diffusion was assumed operative below that altitude.

D. Small-Scale Structure (Less than 10 m)

Small-scale structure includes all irregularities with spatial wavelengths less than the ion gyroradius. In this regime, the collisional Rayleigh-Taylor (not the gradient-drift) instability is applicable. Even the low-frequency collisional drift waves are strongly damped by ion viscosity (Huba and Ossakow, 1979). This regime is, therefore, believed a product of a turbulent cascade process in which wave-wave

coupling is important, and on which the high-frequency drift wave instability might be operative.

An important aspect of the Kwajalein equatorial program was the investigation of small-scale irregularities using backscatter radars. Backscatter measurements of 1-m and 36-cm irregularities with the ALTAIR radar (e.g., Tsunoda et al., 1979; Towle, 1980) were complemented by 11-cm irregularity measurements with the TRADEX radar (Tsunoda, 1980c). These radar investigations provided characterization of both the large-scale structural evolution in space and time (Section III-A) and small-scale irregularity growth and decay.

Initial ALTAIR measurements of ESF backscatter in 1977 led to the realization that these ESF irregularities, with scale sizes smaller than the ion gyroradius, could not be produced by low-frequency drift-wave instabilities [Hudson and Kennel, 1975; Costa and Kelley, 1978(a,b)]. Huba et al. (1978) proposed that the observed small-scale structure is likely produced by a high-frequency drift-wave instability, in particular, the lower-hybrid-drift (LHD) instability. The plasma-density gradients are presumed present at the large-scale end of the irregularity spectrum by the collisional Rayleigh-Taylor instability.

The LHD instability appeared to be linearly unstable under presumably typical ESF conditions. In a sample calculation, Huba et al. (1978) estimated that a gradient scale length, L, of 75 m was required for instability growth. Costa and Kelley (1978) have reported in situ measurements of L less than 75 m. Moreover, the large growth rates of this instability are consistent with observations of sudden onsets of ESF backscatter.

Stabilizing mechanisms for the LHD instability have since been considered and found to impose a plasma-density and altitude threshold on small-scale ESF irregularity growth. Sperling and Goldman (1980) pointed out the importance of electron-ion collisions as a damping mechanism. To illustrate this effect, Sperling and Goldman (1980) used a plasma density of 10^6 el/cm^3 and the plasma description used by Huba et al. (1978) and showed that the LHD instability was linearly stable.

They, of course, pointed out that instability was possible in low-plasma-density regions, such as in plasma bubbles. Huba and Ossakow (1981) also noted that electron-neutral collisions will damp irregularity growth at lower altitudes (below 240 km).

The general preference of ESF backscatter for low-plasma-density regions has been experimentally verified. The spatial coincidence of ESF backscatter with low-plasma-density regions has been shown through comparisons with total electron content measurements (Tsunoda and Towle, 1979; Rino et al., 1981), incoherent-scatter radar measurements (Tsunoda, 1980a,b, 1981; Towle, 1980), and in situ measurements (Szuszczewicz et al., 1980; Kelley et al., 1982; Tsunoda et al., 1982). A preference also for upward-directed, mean plasma-density gradients supports the concept that the process is one of turbulent cascade. The damping of ESF backscatter at low altitudes (below 250 km) has also been noted by Tsunoda et al. (1979) and Huba and Ossakow (1981), supporting the damping effects of electron-neutral collisions on the LHD instability.

The most comprehensive measurements of small-scale ESF structure were made during the Plumex I rocket flight in 1979. Simultaneous measurements were of irregularity structure that spanned five orders of magnitude. In situ measurements inside a high-altitude plasma bubble associated with ESF backscatter revealed that LHD waves were damped (Kelley et al., 1982). On this basis, Kelley et al. (1982) argued that small-scale structure, those smaller than the ion gyroradius, must result from wave-wave coupling and not linear excitation of the LHD instability. Huba and Ossakow (1979) have also proposed that 3-m irregularities, those responsible for Jicamarca radar backscatter, are not linearly excited by low-frequency, collisional drift waves that are heavily damped by ion viscosity. Both results suggest all small-scale irregularities below the ion gyroradius are produced by wave-wave coupling. The role of the LHD instability would then be to reduce the amount of damping in the wavelength regime below about 1 m.

Interpretation of Plumex I results should be viewed in perspective. The measurements within the high-altitude plasma bubble were made during

the decay phase of the backscatter plume. Gradient scale lengths on the order of 50 m, as observed by Costa and Kelley (1978a,b) and Kelley et al. (1982) are probably fairly common during the growth phase of plasma bubbles and backscatter plumes. Using the threshold curves published by Huba and Ossakow (1981), we find that the LHD instability is operative in regions where the plasma density is on the order of 10^4 el/cm^3. Tsunoda et al. (1982) have shown that large backscatter plumes are associated with plasma densities of that magnitude. On this basis, we conclude that LHD waves are linearly excited during the growth phase of backscatter plume (and plasma bubble) evolution.

Once the irregularities are formed, cross-field diffusion primarily controls their decay. Classical diffusion would result in the persistence of irregularities for several hours. ALTAIR measurements have shown, however, that the decay of the backscatter plume is relatively rapid, proceeding at a rate of 5 to 18 dB per 10 min (Tsunoda, 1980). A good example is the decay of the backscatter plume in the bottom panel of Figure 15. The plume on the left side of that panel is also presented in Figure 16, mapped about 30 min later. The decay is evident near the head of the plume. The decay process is further illustrated in Figure 20. The segment of the plume located in the topside F layer dissipates in about 30 min.

Huba and Ossakow (1981) considered diffusion effects on ESF irregularities. They concluded that anomalous diffusion must be occurring, probably through drift-wave turbulence. This process is believed to operate via the universal drift instability or the drift-dissipative instability, at spatial wavelengths less than 1 km, but greater than the ion gyroradius. As these low-frequency drift waves smooth out the existing gradients, the growth rate of the LHD instability is reduced. The high-frequency drift waves are themselves incapable of smoothing gradients. Because diffusive damping is proportional to k^2, dissipation of backscatter-producing irregularities can proceed via classical (or anomalous) diffusion. Anomalous diffusion, however, does not appear capable of dissipating km-scale structures. That is, even with anomalous diffusion, these km-scale irregularities would take eight hours to

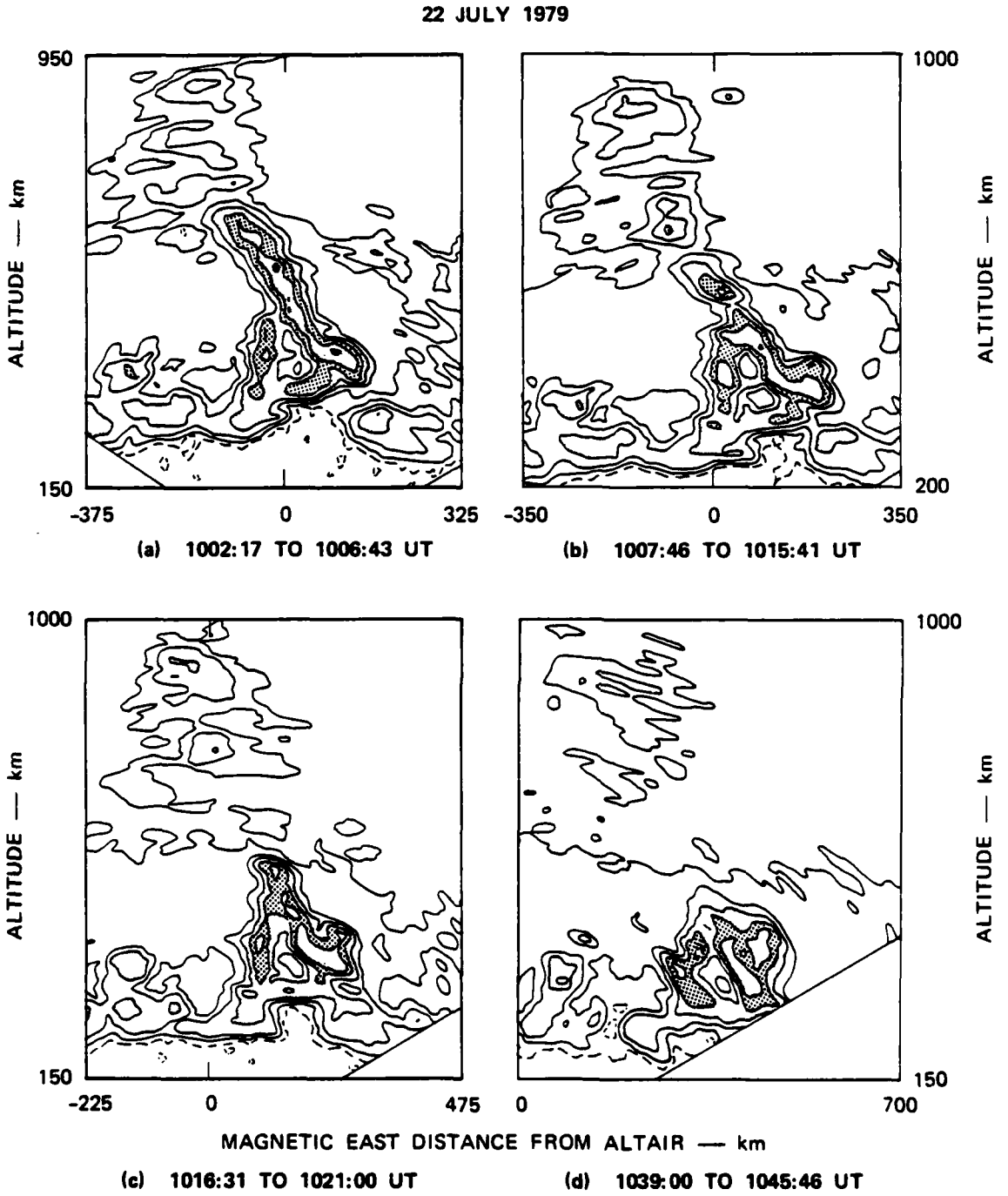

FIGURE 20 SEQUENCE OF ALTAIR BACKSCATTER MAPS SHOWING THE DECAY PHASE OF AN ESF BACKSCATTER PLUME

decay. Huba and Ossakow (1981) proposed that the E-region shorting effects must operate to remove these irregularities.

IV DISCUSSION AND CONCLUSIONS

Late-time (several minutes to many hours after burst), high-altitude nuclear effects are of serious concern to transionospheric communication, navigation, and surveillance systems because of the severe, widespread propagation disturbances that ensue. To mitigate these effects, systems designers must use much higher frequencies or very elaborate coding or equalization schemes or both. Both alternatives are very costly and greatly increase system complexity. Sound decision making among the available options clearly requires accurate phenomenological predictions.

It has been convincingly demonstrated that knowledge of the spectral characteristics of the striations is sufficient for predicting the deleterious effects of propagation disturbances. Thus, it can be argued that the main objective of the phenomenological program is to characterize the temporal and spatial variations of the striation spectrum. Within this broad objective, however, some aspects of the spectral characterization are much more important than others.

The spectral strength in the scale-size regimes that dominate the propagation effects is most important. For frequencies at UHF and below, kilometer-scale and larger structures are most important. At GHz frequencies, subkilometer-scale structures become increasingly more important. It should be kept in mind that under strong-scatter conditions, structures larger than the Fresnel radius dominate the scintillation effects. Of secondary, but not necessarily minor, importance is the spectral shape within the dominant scale-size regime. Any well-defined spectral cutoff is clearly important insofar as extrapolation to higher frequencies is concerned.

The approach that is being used currently in nuclear predictive codes is as follows:

(1) Determine where in a HANE environment convective instabilities are strongly driven.

(2) Estimate the maximum integrated structure level that can occur in the locally unstable volume.

(3) For a specified outer scale wavenumber, distribute the spectral strength according to a k^{-2} power law, down to a specified inner-scale cutoff.

This procedure establishes a reasonable worst case based on our knowledge gleaned from both experiments and theory. On the other hand, the approach depends critically on cutoff wave numbers that we do not as yet fully understand. The ramifications of initial conditions are important as are the diffusive effects that control the evolution and decay of the structure. Thus, continued research is an important adjunct to our current predictive capability.

As discussed in Section III, measurements of ESF phenomena have provided the most detailed characterization of structure development in all the striation scale-size regimes. Indeed, ESF is very regular in its occurrence and characteristics; moreover, the most intense naturally occurring irregularities are found there. Thus, for future applications, ESF phenomena can serve as a systems test bed to demonstrate system performance in a well-defined, reasonably predictable structure environment.

The primary unresolved issues, such as the effects of coupling and large-scale convection patterns, can best be resolved by high-latitude measurements. Moreover, as discussed in Section II, a rich variety of other potentially relevant phenomena occurs in the auroral zone, such as energetic particle precipitation, field-aligned currents, and parallel electric fields. Finally, current phenomenology models cannot make reliable HANE predictions at high latitudes. Thus, future effort will emphasize high-latitude phenomenology heavily.

To summarize, current HANE phenomenological codes made reasonable worst-case predictions of propagation effects. Future research is

needed, however, to refine and extend the predictive capability, particularly where very expensive mitigation schemes are being considered. Naturally occurring striations provide the most readily accessible data resource for verifying our ability to accurately describe the relevant physical processes and their interaction in a large-scale system.

The research reviewed in this report has provided both an extensive data base and a theoretical framework, within which the relevant physical processes can be identified and extrapolated to refine HANE predictions.

REFERENCES

Anderson, D. N. and G. Haerendel, "The Motion of Depleted Plasma Regions in the Equatorial Ionosphere," J. Geophys. Res., 84, 4251 (1979).

Costa, E. and M. C. Kelley, "Linear Theory for the Collisionless Drift Wave Instability with Wavelengths Near the Ion Gyroradius," J. Geophys. Res., 83, 4365 (1978a).

Costa, E. and M. C. Kelley, "On the Role of Steepened Structures and Drift Waves in Equatorial Spread F," J. Geophys. Res., 83(A9), 4359-4364 (1978b).

Dungey, J. W., "Convective Diffusion in the Equatorial F Region," J. Atmos. Terr. Phys., 9, 304 (1956).

Farley, D. T., B. B. Balsley, R. F. Woodman, and J. P. McClure, "Equatorial Spread F: Implications of VHF Radar Observations", J. Geophys. Res., 75, 7199 (1970).

Fremouw, E. J., C. L. Rino, R. C. Livingston, and M. C. Cousins, "A Persistent Subauroral Scintillation Enhancement Observed in Alaska," Geophys. Res. Letts., 4, 539 (1977).

Haerendel, G., "Theory of Equatorial Spread F," preprint, Max-Planck-Institut fur Physik und Astrophysik, Institut fur Extraterrestrische Physik, 8046 Garching, FRG (1973).

Huba, J. D. and S. L. Ossakow, "On the Generation of 3-m Irregularities During Equatorial Spread F by Low-Frequency Drift Waves," J. Geophys. Res., 84, 6697 (1979).

Huba, J. D. and S. L. Ossakow, "Diffusion of Small-Scale Density Irregularities during Equatorial Spread F," J. Geophys. Res., 86, 9107-9114 (1981).

Huba, J. D., P. K. Chaturvedi, S. L. Ossakow, and D. M. Towle, "High-Frequency Drift Waves with Wavelengths Below the Ion Gyroradius in Equatorial Spread F," Geophys. Res. Letts., 5, 695 (1978).

Hudson, M. K. and C. F. Kennel, "Linear Theory of Equatorial Spread F," J. Geophys. Res., 80, 4581 (1975).

Kelley, M. C. and E. Ott, "Two-Dimensional Turbulence in Equatorial Spread F," J. Geophys. Res., 83, 4369 (1978).

Kelley, M. C., J. F. Vickrey, C. W. Carlson, and R. Torbert, "On the Origin and Spatial Extent of High Latitude F Region Irregularities," J. Geophys. Res., 87(A6), (1982).

Keskinen, M. J., S. L. Ossakow, and B. E. McDonald, "Nonlinear Evolution of Diffuse Auroral F Region Ionospheric Irregularities", Geophys. Res. Letts., 7, 573 (1980).

Keskinen, M. J. and S. L. Ossakow, "Nonlinear Evolution of Plasma Enchancements in the Auroral Ionosphere. 1. Long Wavelength Irregularities," J. Geophys. Res., 87(A1), 144-150, (1982).

Linson, L. M. and J. B. Workman, "Formation of Striations in Ionospheric Plasma Clouds," J. Geophys. Res., 75, 3211 (1970).

Livingston, R. C., C. L. Rino, J. P. McClure, and W. B. Hanson, "Spectral Characteristics of Medium-Scale Equatorial F-Region Irregularities," J. Geophys. Res., 86(A4), 2421 (1981).

Livingston, R. C., C. L. Rino, J. Owen, and R. T. Tsunoda, "The Anisotropy of High-Latitude Nighttime F-Region Irregularities," (accepted for publication in J. Geophys. Res., 1982).

Ossakow, S. L., "Reviews of Geophysics and Space Physics Ionospheric Irregularities," Geophys. Res. Letts., 17(4), 521 (1979).

Ossakow, S. L. and P. K. Chaturvedi, "Current Convective Instability in the Diffuse Aurora," Geophys. Res. Letts., 6(4), 322-334 (1979).

Ossakow, S. L., S. T. Zalesak, B. E. McDonald, and P. K. Chaturvedi, "Nonlinear Equatorial Spread F: Dependence on Altitude of the F Peak and Bottomside Background Electron Density Gradient Scale Length," J. Geophys. Res., 84, 17 (1979).

Perkins, F. W. and J. H. Doles, III, "Velocity Shear and the E x B Instability," J. Geophys. Res., 80, 211 (1975).

Rino, C. L. and R. C. Livingston, "On the Analysis and Interpretation of Spaced-Receiver Measurements of Transionospheric Radio Waves," (accepted for publication in Radio Sci., 1982).

Rino, C. L., R. C. Livingston, and S. J. Matthews, "Evidence for Sheet-Like Auroral Ionospheric Irregularities," Geophys. Res. Letts., 5(12), 1034-1043 (1978).

Rino, C. L., R. T. Tsunoda, J. Petriceks, M. C. Kelley, and K. D. Baker, "Simultaneous Borne Beacon and In-Situ Measurements of Equatorial Spread F," J. Geophys. Res., 86, 2411 (1981).

Rino, C. L. and J. F. Vickrey, "Recent Results in Auroral Zone Scintillation Studies," (accepted for publication in J. Atmos. Terr. Phys., (1982).

Scannapieco, A. J. and S. L. Ossakow, "Nonlinear Equatorial Spread F," Geophys. Res. Letts., 3, 451 (1976).

Sipler, D., M. Biondi, and R. Hake, "Optical Studies in Support of the July 1979 Kwajalin Equatorial Spread-F Campaign, Proc. Summer Equatorial Exp. Data Rev. Mtg., 18 March 1980, DNA 5528P, Contract DNA 001-78-C-0379, SRI Project 7745, SRI International, Menlo Park, CA (November 1980).

Sperling, J. L. and S. R. Goldman, "Electron Collisional Effects on Lower Hybrid Drift Instabilities in the Ionosphere," J. Geophys. Res., 85, 3494-3498 (1980).

Szuszczewicz, E. P., R. T. Tsunoda, R. Narcisi, and J. C. Holmes, "Coincident Radar and Rocket Observations of Spread F," Geophys. Res. Letts., 7(7), 537 (1980).

Szuszczewicz, E. P., R. T. Tsunoda, R. Narcisi, and J. C. Holmes, "Plumex II: A Second Set of Coincident Radar and Rocket Observations of Equatorial Spread F," Geophys. Res. Letts., 8, 803-806 (1981).

Towle, D. M., "VHF and UHF Radar Observations of Equatorial Ionospheric Irregularities and Background Densities," Radio Sci., 15, 71-86 (1980).

Tsunoda, R. T., "On the Spatial Relationship of 1-m Equatorial Spread F Irregularities and Plasma Bubbles," J. Geophys. Res., 85(A1), 185 (1980a).

Tsunoda, R. T., "Magnetic-Field Aligned Characteristics of Plasma Bubbles in the Nighttime Equatorial Ionosphere," J. Atmos. Terr. Phys., 42, 743-752 (1980b).

Tsunoda, R. T., "Backscatter Measurements of 11-cm Equatorial Spread-F Irregularities," Geophys. Res. Letts., 7(10), 848-850 (1980c).

Tsunoda, R. T., "Time Evolution and Dynamics of Equatorial Backscatter Plumes. 1. Growth Phase," J. Geophys. Res., 86, 139-149 (1981).

Tsunoda, R. T. and D. M. Towle, "On the Spatial Relationship of 1-Meter Equatorial Spread-F Irregularities and Depletions in Total electron Content," Geophys. Res. Letts., 6, 873 (1979).

Tsunoda, R. T., M. J. Baron, J. Owen, and D. M. Towle, "Altair: An Incoherent-Scatter Radar for Equatorial Spread F Studies," Radio Sci., 14, 1111-1119 (1979).

Tsunoda, R. T., R. C. Livingston, J. P. McClure, and W. B. Hanson, "Equatorial Plasma Bubbles: Vertical-Elongated Wedges from the Bottomside F Layer," (accepted for publication in J. Geophys. Res., 1982).

Tsunoda, R. T., R. C. Livingston, and C. L. Rino, "Evidence of a Velocity Shear in Bulk Plasma Motion Associated with the Postsunset Rise of the Equatorial F Layer," Geophys. Res. Letts., 8, 807-810 (1981).

Tsunoda, R. T. and B. R. White, "On the Generation and Growth of Equatorial Backscatter Plumes. 1. Wave Structure in the Bottomside F Layer," J. Geophys. Res., 86, 3610-3616 (1981).

Vickrey, J. F., "Radar Observations of Structured Plasma in the High-Latitude F Region," Final Report, DNA 564JF, Contract DNA 001-80-C-0015, SRI Project, SRI International, Menlo Park, CA (March 1981).

Vickrey, J. F. and M. C. Kelley, "The Effects of a Conducting E-Layer on Classical F-Region Cross-Field Plasma Diffusion," (accepted for publication in J. Geophys. Res., 1982).

Vickrey, J. F., C. L. Rino, and T. A. Potemra, "Chatanika/Triad Observations of Unstable Ionization Enchancements in the Auroral F-Region," Geophys. Res. Letts., 7(10), 789-792 (1980).

Zalesak, S. T. and S. L. Ossakow, "Nonlinear Equatorial Spread F: Spatially Large Bubbles Resulting From Large Horizontal Scale Initial Perturbations," J. Geophys. Res., 85, 2131-2142 (1980).

Zalesak, S. T., S. L. Ossakow, and P. K. Chaturvedi, "Nonlinear Equatorial Spread F: The Effect of Neutral Winds and Background Pedersen Conductivity," J. Geophys. Res., 87, 151-166 (1982).

DISTRIBUTION LIST

DEPARTMENT OF DEFENSE

Command & Control Technical Center
ATTN: C-312, R. Mason
ATTN: C-650, G. Jones
ATTN: C-650
3 cy ATTN: C-650, W. Heidig

Defense Nuclear Agency
ATTN: STNA
ATTN: NAFD
ATTN: RAEE
ATTN: NATD
ATTN: RAAE, P. Lunn
3 cy ATTN: RAAE
4 cy ATTN: TITL

Defense Technical Information Center
12 cy ATTN: DD

Field Command
Defense Nuclear Agency, Det 1
Lawrence Livermore Lab
ATTN: FC-1

Interservice Nuclear Weapons School
ATTN: TTV

DEPARTMENT OF THE ARMY

BMD Advanced Technology Center
ATTN: ATC-R, W. Dickinson
ATTN: ATC-O, W. Davies
ATTN: ATC-T, M. Capps
ATTN: ATC-R, D. Ross

Harry Diamond Laboratories
ATTN: DELHD-NW-P
ATTN: DELHD-NW-R, R. Williams

US Army Communications Command
ATTN: CC-OPS-WR, H. Wilson
ATTN: CC-OPS-W

US Army Nuclear & Chemical Agency
ATTN: Library

DEPARTMENT OF THE NAVY

Naval Electronic Systems Command
ATTN: Code 501A
ATTN: PME 117-211, B. Kruger
ATTN: PME 106-4, S. Kearney
ATTN: PME 117-2013, G. Burnhart
ATTN: PME 117-20
ATTN: PME 106-13, T. Griffin
ATTN: Code 3101, T. Hughes

Naval Ocean Systems Center
ATTN: Code 532
ATTN: Code 5322, M. P> lson
ATTN: Code 5323, J. He j:son

DEPARTMENT OF THE NAVY (Continued)

Naval Research Laboratory
ATTN: Code 4720, J. Davis
ATTN: Code 7500, B. Wald
ATTN: Code 4780, S. Ossakow
ATTN: Code 4187
ATTN: Code 4700
ATTN: Code 4780
ATTN: Code 6700
ATTN: Code 7950, J. Goodman

Office of Naval Research
ATTN: Code 414, G. Joiner
ATTN: Code 412, W. Condell

Theater Nuclear Warfare Prj Office
ATTN: PM-23, D. Smith

DEPARTMENT OF THE AIR FORCE

Air Force Geophysics Laboratory
ATTN: OPR, H. Gardiner
ATTN: OPR-1
ATTN: LKB, K. Champion
ATTN: CA, A. Stair
ATTN: PHY, J. Buchau
ATTN: R. Babcock
ATTN: R. O'Neil

Air Force Weapons Laboratory
ATTN: SUL
ATTN: NTYC
ATTN: NTN

Air Force Wright Aeronautical Lab
ATTN: W. Hunt
ATTN: A. Johnson

DEPARTMENT OF ENERGY

Department of Energy
GTN
ATTN: DP-233

DEPARTMENT OF ENERGY CONTRACTORS

Los Alamos National Laboratory
ATTN: MS 670, J. Hopkins
ATTN: D. Simons
ATTN: MS 664, J. Zinn
ATTN: T. Kunkle, ESS-5
ATTN: P. Keaton
ATTN: R. Jeffries
ATTN: J. Wolcott

Sandia National Lab
ATTN: Tech Lib 3141
ATTN: Space Project Div
ATTN: D. Dahlgren
ATTN: Org 4231, T. Wright
ATTN: D. Thornbrough
ATTN: Org 1250, W. Brown

DEPARTMENT OF DEFENSE CONTRACTORS

Berkeley Research Associates, Inc
ATTN: J. Workman
ATTN: S. Brecht
ATTN: C. Prettie

Charles Stark Draper Lab, Inc
ATTN: A. Tetewski
ATTN: D. Cox
ATTN: J. Gilmore

EOS Technologies, Inc
ATTN: B. Gabbard

Honeywell, Inc
ATTN: G. Terry, Avionics Dept
ATTN: G. Collyer, Avionics Dept

JAYCOR
ATTN: J. Sperling

Johns Hopkins University
ATTN: J. Newland
ATTN: T. Evans
ATTN: P. Komiske
ATTN: J. Phillips

Kaman Sciences Corp
ATTN: T. Stephens

Kaman Tempo
ATTN: B. Gambill
ATTN: DASIAC
ATTN: J. Devore
ATTN: W. McNamara
ATTN: W. Knapp
ATTN: K. Schwartz

M.I.T. Lincoln Lab
ATTN: D. Towle

Pacific-Sierra Research Corp
ATTN: H. Brode, Chairman SAGE

Physical Dynamics, Inc
ATTN: E. Fremouw

DEPARTMENT OF DEFENSE CONTRACTORS (Continued)

Mission Research Corp
ATTN: F. Fajen
ATTN: R. Hendrick
ATTN: R. Bogusch
ATTN: R. Bigoni
ATTN: C. Lauer
ATTN: S. Gutsche
ATTN: R. Kilb
ATTN: D. Knepp
ATTN: Tech Library
ATTN: G. McCartor
ATTN: F. Guigliano

R&D Associates
ATTN: R. Lelevier
ATTN: W. Karzas
ATTN: W. Wright
ATTN: R. Turco
ATTN: M. Gantsweg
ATTN: C. Greifinger
ATTN: F. Gilmore
ATTN: H. Ory

SRI International
ATTN: V. Gonzales
ATTN: W. Chesnut
ATTN: D. McDaniels
ATTN: M. Baron
ATTN: R. Leadabrand
ATTN: G. Price
ATTN: D. Neilson
ATTN: A. Burns
ATTN: G. Smith
ATTN: J. Petrickes
ATTN: W. Jaye
4 cy ATTN: R. Tsunoda
4 cy ATTN: J. Vickrey
4 cy ATTN: R. Livingston
4 cy ATTN: C. Rino

Visidyne, Inc
ATTN: O. Shepard
ATTN: W. Reidy
ATTN: C. Humphrey
ATTN: J. Carpenter


LM